

H. J. Hall

Shock-Wave Compressions of Twenty-Seven Metals. Equations of State of Metals*

JOHN M. WALSH, MELVIN H. RICE, ROBERT G. MCQUEEN, AND FREDERICK L. YARGER
University of California, Los Alamos Scientific Laboratory, Los Alamos, New Mexico

(Received January 18, 1957)

An explosive system is used to drive a strong shock wave into a plate of 24ST aluminum. This shock wave propagates through the 24ST aluminum into small test specimens which are in contact with the front surface of the plate. A photographic technique is used to measure velocities associated with the 24ST aluminum shock wave and with the shock wave in each specimen.

The measured velocities are transformed, using the conservation relations, to pressure-compression points. Resulting pressure-compression curves are given for 27 metals. The range of data is different for each material but typically covers the pressure interval 150 to 400 kilobars; probable errors in reported experimental pressure-compression curves are 1 or 2% in compression for a given pressure.

The experimental curves, which consist thermodynamically of a known P, V, E locus for each material, are used to calculate a more complete high-pressure equation of state. This is done by means of a theoretical estimate of the volume variation of the Grüneisen ratio $\gamma(V) = V(\partial P / \partial E)_V$. Calculated P, V, T states are listed for the various materials. For 24ST aluminum, quantities of application in shock-wave hydrodynamics are also tabulated.

INTRODUCTION

IN Sec. I an experimental method to obtain dynamic pressure-compression curves for solids is described and resulting data, plotted in Figs. 3-29, are listed for the following 27 solids: beryllium, bismuth, cadmium, chromium, cobalt, copper, gold, iron, lead, magnesium, molybdenum, nickel, silver, thorium, tin, titanium, zinc, 24ST aluminum, brass, indium, niobium, palladium, platinum, rhodium, tantalum, thallium, and zirconium.

Section II is devoted to the problem of generalizing the experimental Hugoniot curves into a complete thermodynamic description of high pressure states neighboring the experimental curves.

Throughout the present discussion it is assumed that stresses behind the shock wave are isotropic, and that the compressed materials behind the shock wave are in thermodynamic equilibrium. Further discussion of basic principles underlying the present work is found in pre-

vious papers^{1,2} dealing with dynamic pressure-compression results.

I. DETERMINATION OF HUGONIOT CURVES

A. Measurement of Shock Wave and Free-Surface Velocities

The experimental method used to measure shock wave and free-surface velocities is illustrated in Fig. 1. The detonation of the explosive system, pictured at the top of the figure, causes a plane shock wave to be transmitted into the 24ST aluminum plate. This shock wave next interacts with the test specimen, Lucite, iron-shim assembly on the front surface of the plate. The essential features of this assembly are the two rows of test pellets and the 0.003-in. thick argon-filled flash gaps. The pellets consist of one row of five thick specimens (0.250 in. thick by 0.750 in. diameter) to provide for shock velocity measurements and one row of thin specimens (0.125 in. thick by 0.750 in. diameter) for

* Work done under the auspices of the U. S. Atomic Energy Commission.

¹ J. M. Walsh and R. H. Christian, *Phys. Rev.* **97**, 1544 (1955).

² Goranson, Bancroft, Burton, Blechar, Houston, Gittings, and Landeen, *J. Appl. Phys.* **26**, 1472 (1955).

free-surface velocity measurements of the same five materials. The flash gaps, when closed by the shock wave, provide light (due to multiple shock reflections in the argon) which is recorded by a moving image camera. The camera, in an underground bunker some 15 feet from the shot assembly, views the assembly through a slit system and sweeps the image in a direction normal to the slits.

A photographic record is also seen in Fig. 1, where

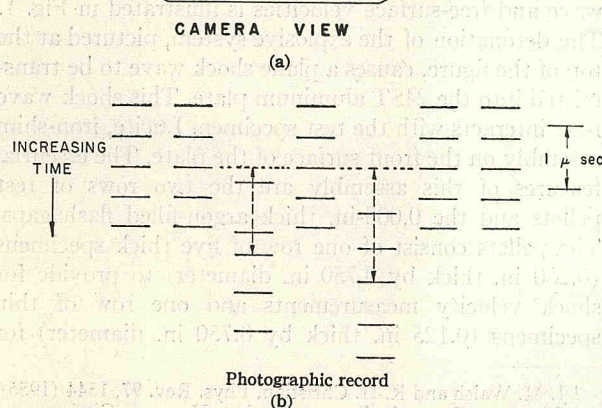
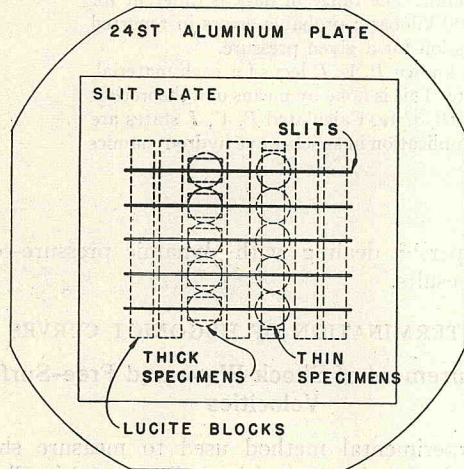
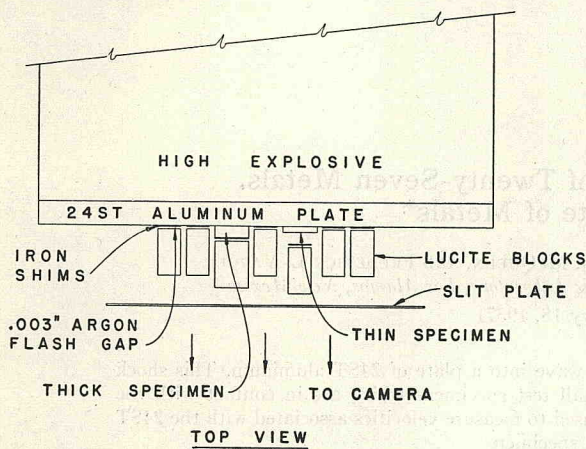


FIG. 1. Drawing of sweep camera photographic record.

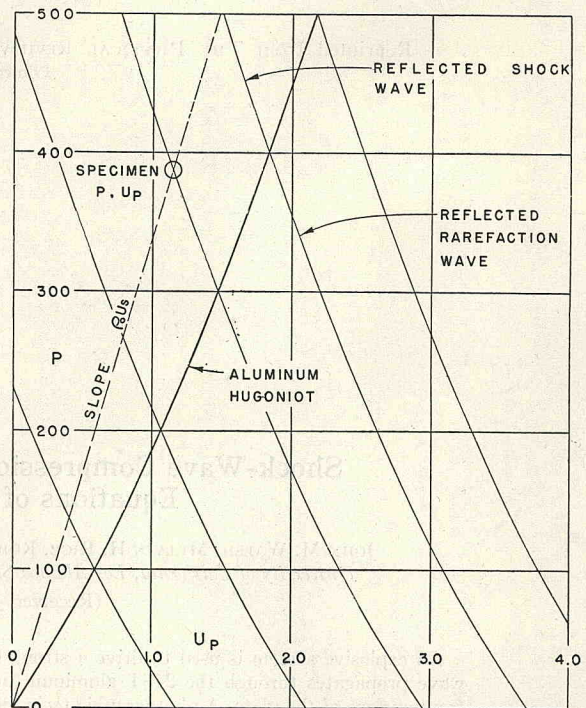


FIG. 2. Pressure versus particle velocity curves for 24ST aluminum, and a typical graphical solution to determine P , U_p for a test specimen.

pertinent features are identified. The record is analyzed by comparator reading, measured record offsets being converted to times by use of the known camera sweep speed. The measured time³ offset for the thick pellet is divided into pellet thickness to give the shock wave velocity for that material. The measured time for the thin pellet of the same material is the shock wave transit time through the thin pellet plus the time required for the free surface to traverse the free-run distance. When combined with the measured shock wave velocity and the known free-run distance, it gives the desired free-surface velocity. The measured shock wave and free-surface velocities are listed in Table I, second and third columns.

B. Transformation of Measured Velocities to Pressure-Volume Points

The transformation of measured velocities to pressure-compression points is done by two methods, both of

³ Small corrections are incorporated into the measured time offsets. These corrections arise from the fact that the 0.003-in. argon flash gaps over test specimen are closed at different velocities from the flash gaps over the main 24ST aluminum plate. The magnitude of each correction is determined by solution of the appropriate interface problems, using the graphical pressure-particle velocity method discussed below. The applied corrections are taken to be the total difference in flash-gap closure times from the assumption that the light flash occurs in the final stages of closure of the flash gap. The corrections seldom affect measured velocities more than 0.5%, and more typically cause a change of about 0.2%.

TABLE I. Experimental data.

| Metal | Shock wave velocity U_s (km/sec) | Free surface velocity U_{fs} (km/sec) | Free surface approximation | | Graphical solution | | |
|---|--|---|-------------------------------|----------------------------|--|-------------------------------|----------------------------|
| | | | Pressure P (kilobars) | Relative volume V/V_0 | Shock particle velocity U_p (km/sec) | Pressure P (kilobars) | Relative volume V/V_0 |
| Beryllium | 9.044 | 1.697 | 141.6 | 0.9062 | 0.847 | 141.3 | 0.9063 |
| $\rho_0 = 1.845 \text{ g/cm}^3$ | 8.934 | 1.739 | 143.3 | 0.9027 | 0.865 | 142.6 | 0.9032 |
| $C_p = 0.474 \text{ cal/g } ^\circ\text{C}$ | 9.112 | 2.358 | 198.2 | 0.8706 | 1.189 | 199.9 | 0.8695 |
| $\frac{1}{V} \left(\frac{\partial V}{\partial T} \right)_p = 37 \times 10^{-6} / ^\circ\text{C}$ | 9.332 | 2.364 | 203.5 | 0.8733 | 1.221 | 210.2 | 0.8692 |
| | 9.851 | 3.422 | 311.0 | 0.8263 | 1.730 | 314.4 | 0.8244 |
| | 9.832 | 3.235 | 293.4 | 0.8355 | 1.609 | 291.9 | 0.8364 |
| | 9.633 | 3.189 | 283.4 | 0.8345 | 1.592 | 282.9 | 0.8347 |
| Bismuth | 2.696 | 1.401 | 184.9 | 0.7402 | 0.718 | 189.5 | 0.7337 |
| $\rho_0 = 9.79 \text{ g/cm}^3$ | 2.585 | 1.318 | 166.8 | 0.7451 | 0.676 | 171.1 | 0.7385 |
| $C_p = 0.293 \text{ cal/g } ^\circ\text{C}$ | 3.075 | 1.793 | 269.9 | 0.7085 | 0.914 | 275.2 | 0.7028 |
| $\frac{1}{V} \left(\frac{\partial V}{\partial T} \right)_p = 40 \times 10^{-6} / ^\circ\text{C}$ | 3.084 | 1.800 | 271.7 | 0.7082 | 0.922 | 278.4 | 0.7010 |
| | 3.682 | 2.476 | 446.3 | 0.6638 | 1.212 | 436.9 | 0.6708 |
| | 3.659 | 2.564 | 459.2 | 0.6496 | 1.222 | 437.7 | 0.6660 |
| Cadmium | 3.599 | 1.464 | 227.5 | 0.7966 | 0.690 | 214.4 | 0.8083 |
| $\rho_0 = 8.64 \text{ g/cm}^3$ | 3.421 | 1.277 | 188.6 | 0.8134 | 0.619 | 182.9 | 0.8191 |
| $C_p = 0.055 \text{ cal/g } ^\circ\text{C}$ | 3.918 | 1.757 | 297.2 | 0.7758 | 0.850 | 287.6 | 0.7830 |
| $\frac{1}{V} \left(\frac{\partial V}{\partial T} \right)_p = 89.4 \times 10^{-6} / ^\circ\text{C}$ | 4.450 | 2.496 | 479.6 | 0.7196 | 1.190 | 457.3 | 0.7326 |
| | 4.324 | 2.400 | 448.1 | 0.7225 | 1.120 | 418.2 | 0.7410 |
| Chromium | 6.043 | | | | 0.5448 | 234.5 | 0.9098 |
| $\rho_0 = 7.13$ | 5.923 | | | | 0.5395 | 233 | 0.9089 |
| $C_p = 0.065$ | 6.381 | | | | 0.7436 | 338 | 0.8835 |
| $\frac{1}{V} \left(\frac{\partial V}{\partial T} \right)_p = 18.6 \times 10^{-6} / ^\circ\text{C}$ | 6.370 | | | | 0.7449 | 338 | 0.8831 |
| | 6.355 | | | | 0.7407 | 336 | 0.8834 |
| | 6.357 | | | | 0.7403 | 336 | 0.8835 |
| | 6.660 | | | | 1.007 | 478 | 0.8488 |
| | 6.674 | | | | 1.008 | 479 | 0.8490 |
| Cobalt | 5.445 | 1.016 | 244.0 | 0.9067 | 0.502 | 241.1 | 0.9078 |
| $\rho_0 = 8.82$ | 5.696 | 1.327 | 333.4 | 0.8835 | 0.683 | 343.2 | 0.8801 |
| $C_p = 0.099$ | 5.632 | 1.334 | 331.4 | 0.8816 | 0.653 | 324.4 | 0.8841 |
| $\frac{1}{V} \left(\frac{\partial V}{\partial T} \right)_p = 36.9 \times 10^{-6} / ^\circ\text{C}$ | 6.019 | ... | ... | ... | 0.901 | 478.1 | 0.8503 |
| | 6.052 | 1.890 | 504.5 | 0.8439 | 0.955 | 509.8 | 0.8422 |
| Copper | 4.744 | 1.024 | 216.2 | 0.8921 | 0.511 | 215.8 | 0.8923 |
| $\rho_0 = 8.90$ | 4.768 | 1.094 | 232.1 | 0.8853 | 0.570 | 241.9 | 0.8804 |
| $C_p = 0.092$ | 5.070 | 1.440 | 324.9 | 0.8580 | 0.711 | 320.8 | 0.8598 |
| $\frac{1}{V} \left(\frac{\partial V}{\partial T} \right)_p = 49.5 \times 10^{-6} / ^\circ\text{C}$ | 5.015 | 1.456 | 324.9 | 0.8548 | 0.731 | 326.3 | 0.8542 |
| | 5.508 | 2.079 | 509.6 | 0.8113 | 1.032 | 505.9 | 0.8126 |
| Gold | 3.679 | 0.771 | 272.9 | 0.8952 | 0.380 | 269.0 | 0.8967 |
| $\rho_0 = 19.24$ | 3.864 | 1.012 | 376.2 | 0.8690 | 0.505 | 375.4 | 0.8693 |
| $C_p = 0.312$ | 4.130 | 1.375 | 546.3 | 0.8335 | 0.666 | 529.2 | 0.8389 |
| $\frac{1}{V} \left(\frac{\partial V}{\partial T} \right)_p = 42.6 \times 10^{-6} / ^\circ\text{C}$ | | | | | | | |
| Iron | 5.652 | 2.163 | 479.2 | 0.8087 | 1.085 | 480.8 | 0.8080 |
| $\rho_0 = 7.84$ | 5.474 | 2.037 | 437.1 | 0.8139 | 1.013 | 434.7 | 0.8149 |
| $C_p = 0.107$ | 5.458 | 1.988 | 425.3 | 0.8179 | 0.993 | 424.9 | 0.8181 |
| $\frac{1}{V} \left(\frac{\partial V}{\partial T} \right)_p = 35.1 \times 10^{-6} / ^\circ\text{C}$ | 5.438 | 2.005 | 427.4 | 0.8156 | 0.994 | 423.8 | 0.8172 |
| | 5.229 | 1.789 | 366.7 | 0.8289 | ... | ... | ... |
| | 5.231 | 1.773 | 363.6 | 0.8305 | ... | ... | ... |
| | 5.206 | 1.755 | 358.2 | 0.8314 | ... | ... | ... |
| | 5.209 | 1.755 | 358.4 | 0.8315 | ... | ... | ... |
| Lead | 2.914 | 1.230 | 203.0 | 0.7889 | 0.590 | 194.8 | 0.7975 |
| $\rho_0 = 11.34$ | 3.268 | 1.745 | 323.1 | 0.7330 | 0.819 | 303.2 | 0.7494 |
| $C_p = 0.030$ | 3.250 | 1.731 | 318.7 | 0.7337 | 0.802 | 295.3 | 0.7532 |
| $\frac{1}{V} \left(\frac{\partial V}{\partial T} \right)_p = 85.1 \times 10^{-6} / ^\circ\text{C}$ | 3.724 | 2.420 | 510.5 | 0.6751 | 1.118 | 471.7 | 0.6998 |
| Magnesium | 5.987 | 2.242 | 116.4 | 0.8128 | | | |
| $\rho_0 = 1.735$ | 7.082 | 4.157 | 260.4 | 0.7066 | | | |
| $C_p = 0.250$ | | | | | | | |
| $\frac{1}{V} \left(\frac{\partial V}{\partial T} \right)_p = 76.8 \times 10^{-6} / ^\circ\text{C}$ | | | | | | | |

TABLE I.—Continued.

| Metal | Shock wave velocity U_s (km/sec) | Free surface velocity U_{fs} (km/sec) | Free surface approximation | | Shock particle velocity U_p (km/sec) | Graphical solution | |
|--|---|---|-------------------------------|----------------------------|--|-------------------------------|----------------------------|
| | | | Pressure P (kilobars) | Relative volume V/V_0 | | Pressure P (kilobars) | Relative volume V/V_0 |
| Molybdenum | 5.699 | 0.874 | 254.0 | 0.9233 | 0.437 | 254.0 | 0.9233 |
| $\rho_0=10.20$ | 5.647 | 0.888 | 255.7 | 0.9214 | 0.444 | 255.2 | 0.9214 |
| $C_p=0.0612$ | 5.955 | 1.176 | 357.2 | 0.9013 | 0.591 | 359.0 | 0.9008 |
| $\frac{1}{V}\left(\frac{\partial V}{\partial T}\right)_p = 15 \times 10^{-6}/^\circ\text{C}$ | 5.861 | 1.200 | 358.7 | 0.8976 | 0.606 | 362.3 | 0.8966 |
| | 6.210 | 1.724 | 546.0 | 0.8612 | 0.850 | 538.4 | 0.8631 |
| | 6.124 | 1.636 | 511.0 | 0.8664 | 0.792 | 494.7 | 0.8707 |
| Nickel | 5.417 | 0.981 | 235.3 | 0.9095 | 0.490 | 235.0 | 0.9095 |
| $\rho_0=8.86$ | 5.653 | 1.350 | 337.8 | 0.8806 | 0.678 | 339.4 | 0.8801 |
| $C_p=0.1050$ | 5.620 | 1.390 | 345.8 | 0.8763 | 0.687 | 341.8 | 0.8778 |
| $\frac{1}{V}\left(\frac{\partial V}{\partial T}\right)_p = 39 \times 10^{-6}/^\circ\text{C}$ | 6.031 | 1.955 | 522.0 | 0.8379 | 0.957 | 511.0 | 0.8413 |
| | 5.969 | 1.981 | 523.5 | 0.8341 | 0.982 | 519.0 | 0.8355 |
| | 5.952 | 1.835 | 483.5 | 0.8459 | 0.887 | 467.4 | 0.8510 |
| Silver | 4.065 | 1.015 | 216.4 | 0.8752 | 0.504 | 214.9 | 0.8760 |
| $\rho_0=10.49$ | 4.113 | 1.049 | 226.3 | 0.8725 | 0.527 | 227.4 | 0.8719 |
| $C_p=0.056$ | 4.378 | 1.448 | 332.5 | 0.8346 | 0.717 | 329.3 | 0.8362 |
| $\frac{1}{V}\left(\frac{\partial V}{\partial T}\right)_p = 56.7 \times 10^{-6}/^\circ\text{C}$ | 4.846 | 2.041 | 518.8 | 0.7894 | 0.985 | 500.7 | 0.7967 |
| | 4.848 | 2.074 | 527.4 | 0.7861 | 1.010 | 513.6 | 0.7917 |
| Thorium | 3.497 | 2.112 | 431.3 | 0.6980 | 1.043 | 426.0 | 0.7017 |
| $\rho_0=11.68$ | 3.192 | 1.604 | 299.0 | 0.7487 | 0.812 | 302.7 | 0.7456 |
| $C_p=0.030$ | 2.954 | 1.246 | 215.0 | 0.7891 | 0.620 | 213.9 | 0.7901 |
| $\frac{1}{V}\left(\frac{\partial V}{\partial T}\right)_p = 33.3 \times 10^{-6}/^\circ\text{C}$ | 2.900 | 1.198 | 202.9 | 0.7934 | 0.571 | 193.4 | 0.8031 |
| Tin | 4.555 | 2.704 | 448.3 | 0.7032 | 1.290 | 427.8 | 0.7168 |
| $\rho_0=7.28$ | 4.435 | 2.539 | 409.9 | 0.7138 | 1.190 | 384.2 | 0.7317 |
| $C_p=0.054$ | 4.004 | 1.912 | 278.7 | 0.7612 | 0.925 | 269.6 | 0.7690 |
| $\frac{1}{V}\left(\frac{\partial V}{\partial T}\right)_p = 60 \times 10^{-6}/^\circ\text{C}$ | 3.557 | 1.486 | 192.4 | 0.7911 | 0.705 | 182.6 | 0.8018 |
| | 3.524 | 1.364 | 175.0 | 0.8065 | 0.670 | 171.9 | 0.8098 |
| Titanium | 6.329 | 2.723 | 388.1 | 0.7849 | 1.370 | 390.8 | 0.7835 |
| $\rho_0=4.51$ | 5.790 | 1.926 | 251.3 | 0.8337 | 0.980 | 255.7 | 0.8307 |
| $C_p=0.126$ | 5.501 | 1.437 | 178.1 | 0.8694 | 0.723 | 179.3 | 0.8686 |
| $\frac{1}{V}\left(\frac{\partial V}{\partial T}\right)_p = 25.5 \times 10^{-6}/^\circ\text{C}$ | 5.469 | 1.364 | 168.1 | 0.8753 | 0.684 | 168.6 | 0.8749 |
| Zinc | 5.014 | 2.589 | 463.1 | 0.7418 | 1.250 | 447 | 0.7507 |
| $\rho_0=7.135$ | 4.870 | Zinc single-crystal experiment. See Sec. I-D | | | 1.190 | 414 | 0.7556 |
| $C_p=0.092$ | 4.481 | 1.795 | 286.9 | 0.7997 | 0.88 | 281.4 | 0.8036 |
| $\frac{1}{V}\left(\frac{\partial V}{\partial T}\right)_p = 100 \times 10^{-6}/^\circ\text{C}$ | 4.450 | 1.826 | 289.9 | 0.7948 | 0.894 | 283.9 | 0.7991 |
| | 4.465 | 1.823 | 290.4 | 0.7959 | | | |
| | 4.053 | 1.355 | 195.9 | 0.8328 | 0.650 | 188.0 | 0.8396 |
| | 4.059 | 1.345 | 194.8 | 0.8343 | | | |
| | 4.13 | Zinc single-crystal experiment. See Sec. I-D | | | 0.673 | 198.3 | 0.8370 |
| | 4.022 | 1.295 | 185.8 | 0.8390 | 0.630 | 180.8 | 0.8434 |
| | 4.029 | 1.310 | 188.3 | 0.8374 | | | |
| 24ST aluminum | 7.531 | 3.230 | 335.8 | 0.7874 | | | |
| $\rho_0=2.785$ | 6.927 | 2.319 | 222.7 | 0.8333 | | | |
| $C_p=0.23$ | 6.500 | 1.700 | 153.5 | 0.8696 | | | |
| $\frac{1}{V}\left(\frac{\partial V}{\partial T}\right)_p = 69.0 \times 10^{-6}/^\circ\text{C}$ | | | | | | | |
| | Actual 24ST aluminum data consists of approximately one-hundred points of which the above three are representative. | | | | | | |
| Brass | 4.446 | 1.181 | 220.9 | 0.8672 | 0.590 | 220.7 | 0.8673 |
| $\rho_0=8.413$ | 4.440 | 1.143 | 213.5 | 0.8713 | 0.571 | 213.3 | 0.8714 |
| $C_p=0.09$ | 4.731 | 1.553 | 309.1 | 0.8359 | 0.791 | 314.8 | 0.8328 |
| $\frac{1}{V}\left(\frac{\partial V}{\partial T}\right)_p = 61.6 \times 10^{-6}/^\circ\text{C}$ | 4.726 | 1.569 | 311.9 | 0.8340 | 0.770 | 306.2 | 0.8371 |
| | 5.236 | 2.200 | 484.6 | 0.7899 | 1.085 | 478.0 | 0.7928 |
| | 5.220 | ... | ... | ... | 1.077 | 473.0 | 0.7937 |
| Indium | 3.745 | | | | 0.7837 | 213.5 | 0.7907 |
| $\rho_0=7.27$ | 3.965 | | | | 0.9812 | 283 | 0.7525 |
| $C_p=0.057$ | 4.348 | | | | 1.281 | 405 | 0.7054 |
| $\frac{1}{V}\left(\frac{\partial V}{\partial T}\right)_p = 99 \times 10^{-6}/^\circ\text{C}$ | | | | | | | |

TABLE I.—Continued.

| Metal | Shock wave velocity U_s (km/sec) | Free surface velocity U_{fs} (km/sec) | Free surface approximation | | Graphical solution | | |
|---|--|---|-------------------------------|----------------------------|--|-------------------------------|----------------------------|
| | | | Pressure P (kilobars) | Relative volume V/V_0 | Shock particle velocity U_p (km/sec) | Pressure P (kilobars) | Relative volume V/V_0 |
| Niobium | 5.177 | | | | 0.5489 | 244.5 | 0.8940 |
| $\rho_0 = 8.604$ | 5.311 | | | | 0.7434 | 341 | 0.8606 |
| $C_p = 0.065$ | 5.642 | | | | 0.9929 | 482 | 0.8240 |
| $\frac{1}{V} \left(\frac{\partial V}{\partial T} \right)_p = 23.3 \times 10^{-6}/^\circ\text{C}$ | | | | | | | |
| Palladium | 4.673 | | | | 0.4728 | 262.5 | 0.8988 |
| $\rho_0 = 11.95$ | 5.004 | | | | 0.6200 | 372 | 0.8761 |
| $C_p = 0.0583$ | 5.374 | | | | 0.8219 | 531 | 0.8471 |
| $\frac{1}{V} \left(\frac{\partial V}{\partial T} \right)_p = 35 \times 10^{-6}/^\circ\text{C}$ | | | | | | | |
| Platinum | 4.199 | | | | 0.329 | 295 | 0.9238 |
| $\rho_0 = 21.37$ | 4.306 | | | | 0.4550 | 416.5 | 0.8943 |
| $C_p = 0.0322$ | 4.495 | | | | 0.6102 | 586 | 0.8642 |
| $\frac{1}{V} \left(\frac{\partial V}{\partial T} \right)_p = 26.7 \times 10^{-6}/^\circ\text{C}$ | | | | | | | |
| Rhodium | 5.470 | | | | 0.4100 | 278.5 | 0.9250 |
| $\rho_0 = 12.42$ | 5.865 | | | | 0.7566 | 551 | 0.8710 |
| $C_p = 0.059$ | | | | | | | |
| $\frac{1}{V} \left(\frac{\partial V}{\partial T} \right)_p = 25 \times 10^{-6}/^\circ\text{C}$ | | | | | | | |
| Tantalum | 3.811 | | | | 0.4327 | 271.5 | 0.8865 |
| $\rho_0 = 16.46$ | 4.010 | | | | 0.5800 | 383 | 0.8554 |
| $C_p = 0.034$ | 4.323 | | | | 0.7685 | 547 | 0.8222 |
| $\frac{1}{V} \left(\frac{\partial V}{\partial T} \right)_p = 19.5 \times 10^{-6}/^\circ\text{C}$ | | | | | | | |
| Thallium | 2.804 | | | | 0.6416 | 213 | 0.7712 |
| $\rho_0 = 11.84$ | 2.817 | | | | 0.6386 | 213 | 0.7733 |
| $C_p = 0.031$ | 3.120 | | | | 0.8446 | 312 | 0.7293 |
| $\frac{1}{V} \left(\frac{\partial V}{\partial T} \right)_p = 114 \times 10^{-6}/^\circ\text{C}$ | 3.145 | | | | 0.8406 | 313 | 0.7327 |
| | 3.538 | | | | 1.090 | 456.5 | 0.6919 |
| | 3.541 | | | | 1.089 | 456.5 | 0.6925 |
| Zirconium | 4.494 | | | | 0.7117 | 207.5 | 0.8416 |
| $\rho_0 = 6.49$ | 4.674 | | | | 0.9563 | 290 | 0.7954 |
| $C_p = 0.068$ | 4.920 | | | | 1.275 | 407 | 0.7408 |
| $\frac{1}{V} \left(\frac{\partial V}{\partial T} \right)_p = 15.6 \times 10^{-6}/^\circ\text{C}$ | | | | | | | |

which use the Rankine-Hugoniot relations

$$V/V_{0H} = (U_s - U_p)/U_s, \quad (1)$$

$$P_H = \rho_0 U_s U_p + P_{0H}, \quad (2)$$

for the conservations of mass and momentum across a shock front. Here P_{0H} , V_{0H} refer to pressure and specific volume for the undisturbed state ahead of the shock front and P_H , V denote pressure and specific volume for the state behind the shock front. U_s and U_p are, respectively, the shock wave velocity, and the particle velocity for the state behind the shock front, each relative to the undisturbed state ahead of the shock front.

For the first transformation method, we note that the experimental free-surface velocity, U_{fs} , is the sum

of the shock particle velocity and the particle velocity, U_r , due to the centered rarefaction wave which relieves the pressure, i.e.,

$$U_{fs} = U_p + U_r. \quad (3)$$

The approximate relation⁴ $U_r/U_p \approx 1$, or equivalently

$$U_p \approx U_{fs}/2, \quad (4)$$

is combined with Eqs. (1), (2), and measured values of U_s and U_{fs} to determine pressure-volume points. Resulting data are listed in Table I under *Free Surface Approximation* and are plotted in Figs 3–29 as \times 's.

⁴ Calculated refinements of the free-surface velocity approximation are discussed in Sec. II-B and listed in Table VII. The approximation was also discussed in reference 1, where expressions for possible errors associated with its use were shown to be small.

The second transformation method makes use of certain equation of state data for 24ST aluminum. The necessary 24ST aluminum data (derived using experimental 24ST aluminum results in the next section of this paper) are the curves of pressure *versus* particle velocity shown in Fig. 2. The curve from the origin is the locus of all pressure-particle velocity states attainable by propagating a right-going shock wave into normal undisturbed 24ST aluminum at $P=0$, $U_p=0$. When such a shock wave interacts with the 24ST aluminum-specimen interface, a left-going disturbance is reflected into the aluminum. The locus of P , U_p states that can be reached by the reflected disturbance is given by the appropriate cross curve in Fig. 2. For pressures greater (and particle velocities smaller) than that corresponding to the initial right-going shock wave, the cross curve corresponds to reflected shock waves. For smaller pressures (and greater particle velocities) the cross curve corresponds to a rarefaction wave which is reflected leftward from the interface. The $P=0$ point on each cross curve, in particular, corresponds to the aluminum free-surface velocity for that shock strength.

For the procedure below, it is necessary to identify the cross curve corresponding to the shock wave in the 24ST aluminum plate. This information is obtained by

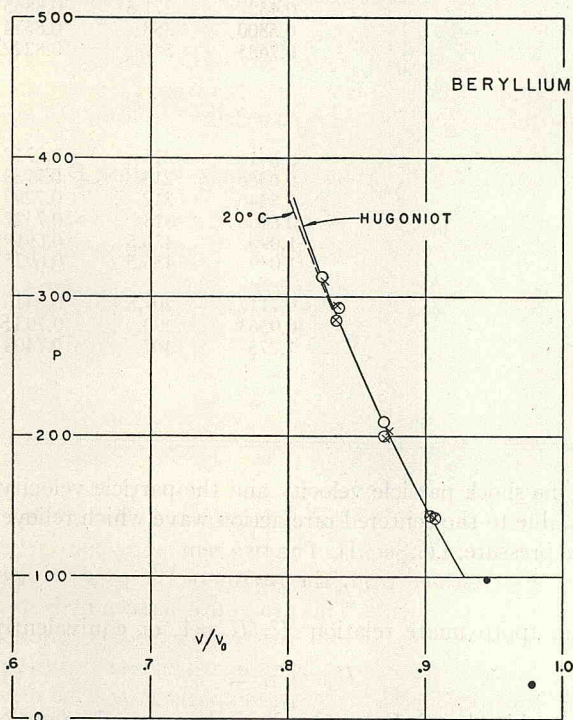


FIG. 3. Pressure-compression curves for beryllium. The solid curve in this figure and in Figs. 4 to 29 is an analytical fit (Table II) of Hugoniot curve experimental data obtained by the graphical solution method. Points plotted as circles in these figures are from the graphical solution method; points plotted as X's are from the free-surface approximation method. (See Sec. IB.) The dashed curve in each figure is a 20°C isotherm, computed using the Hugoniot curve and the methods given in Sec. II. Data points below 100 kilobars are from recent articles by P. W. Bridgman.

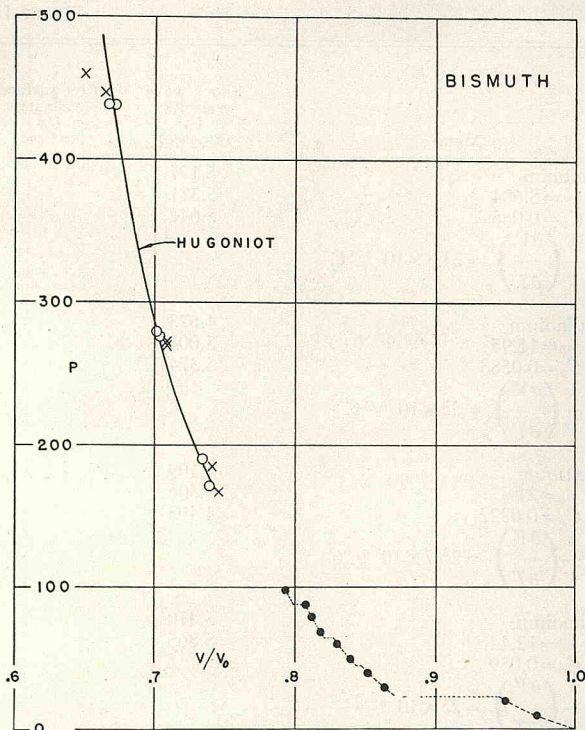


FIG. 4. Pressure-compression curves for bismuth. See caption to Fig. 3.

including a pair of 24ST pellets among the test specimens in each shot. The measured free-surface velocity then identifies the desired cross curve from its intercept with the particle velocity axis. Similarly, the measured shock wave velocity is used to construct a line from the origin in Fig. 2 of slope $\rho_0 U_s$, whose intercept with the above-described locus of right-going shocks determines [see Eq. (1) for $P_0 \approx 0$] the (P, U_p) point for the aluminum shock wave, and consequently determines the associated cross curve. The two determinations of the cross curve are averaged to give the value used in the succeeding analysis.

The boundary conditions that pressure and particle velocity must be continuous across the interface between the 24ST aluminum and the test specimen can now be used to construct a graphical solution. First, the known initial density ρ_0 and the measured shock velocity U_s for each specimen are used to construct a line from the origin (see Fig. 3) of slope $\rho_0 U_s$. From Eq. (1), for $P_0 \approx 0$, it is seen that the desired (P, U_p) point for the shock lies on this ray. The intersection of this ray with the aluminum cross curve then satisfies the boundary conditions and gives the desired pressure and particle velocity. The associated relative volume is then calculated by substituting this particle velocity and the measured shock velocity, U_s , into Eq. (2). Pressure-volume points determined by this method are listed under *Graphical Solutions* in Table I and are plotted in Figs. 3-29 as circles.

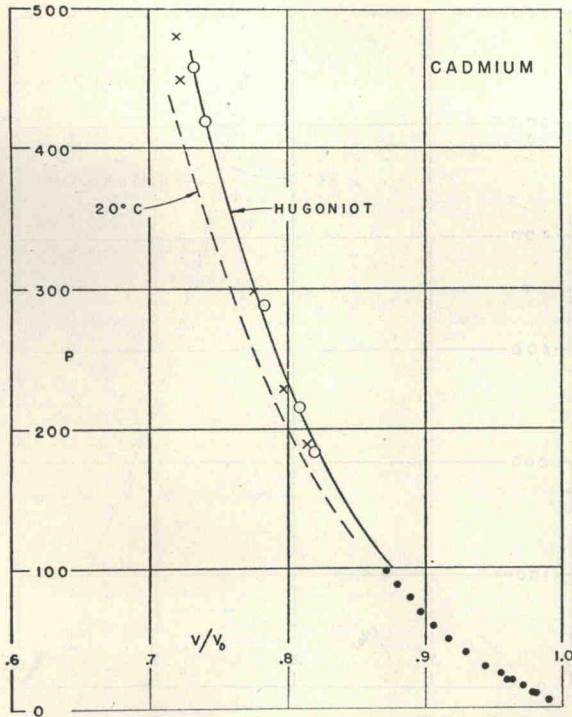


FIG. 5. Pressure-compression curves for cadmium.
See caption to Fig. 3.

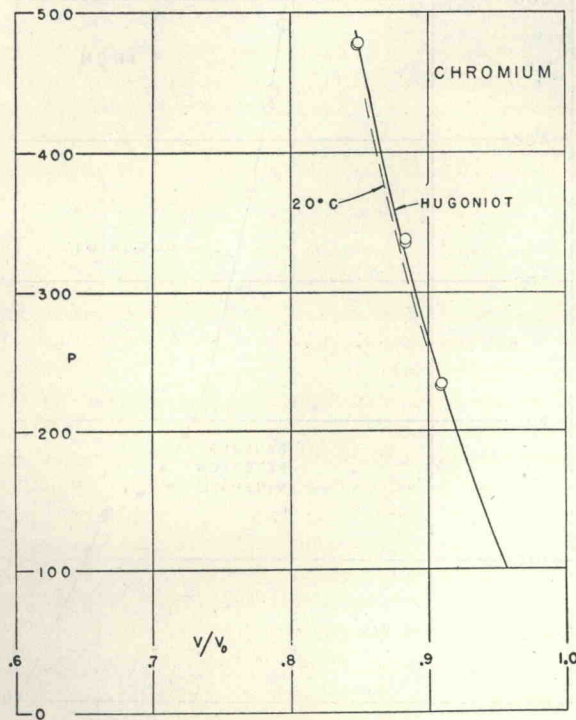


FIG. 6. Pressure-compression curves for chromium.
See caption to Fig. 3.

A few of the experiments reported in Table I were done without free-surface velocity measurements, so that only graphical solutions are listed. Iron and mag-

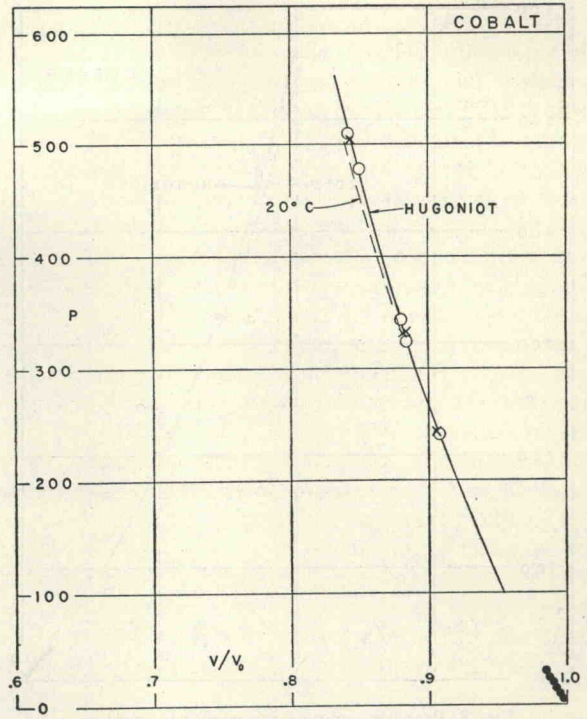


FIG. 7. Pressure-compression curves for cobalt.
See caption to Fig. 3.

nesium experiments were performed without 24ST aluminum backer plates, so that only free-surface approximation solutions are reported.

C. Analytical Fits of Pressure-Volume Data

The Hugoniot curves which are drawn through the experimental points in Figs. 3-29 are reproduced by analytical fits of the form

$$P_H = A\mu + B\mu^2 + C\mu^3, \quad (5)$$

where

$$\mu \equiv (\rho/\rho_0) - 1 = (V_{0H}/V) - 1.$$

The values of A , B , and C for the various solids are listed in Table II. In reality this is a two-parameter fit, since the ratio B/A is determined theoretically by a method given in Sec. II. The two remaining parameters are then selected to fit the results of the present high-pressure experiments. This procedure, as seen by inspection of the figures, gives a satisfactory fit of the present data, and it also forms a standardized extrapolation procedure from which rough comparisons will be made with the lower pressure data from static experimentation.

Finally, from the third mechanical conservation relation

$$E_H - E_{0H} = \frac{1}{2}(P_H + P_{0H})(V_{0H} - V), \quad (6)$$

it is seen that the specific internal energy E_H relative

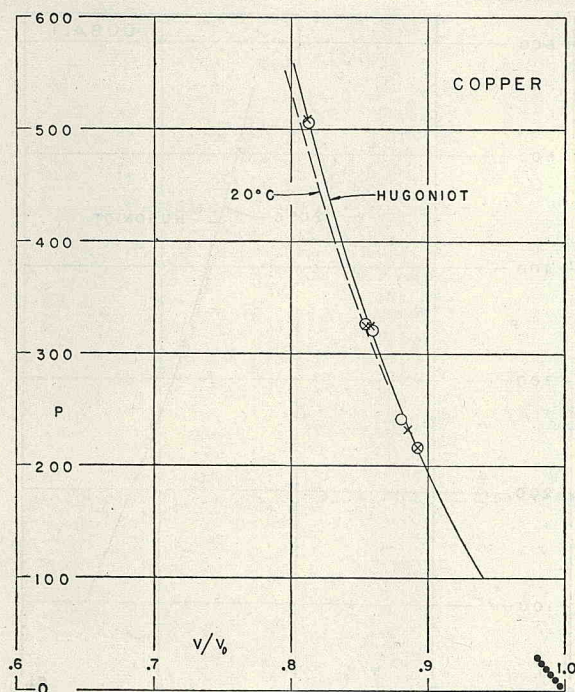


FIG. 8. Pressure-compression curves for copper.
See caption to Fig. 3.

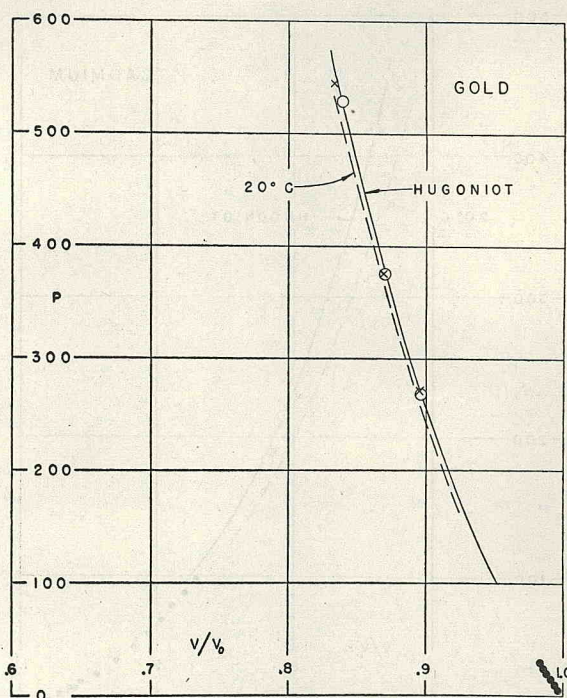


FIG. 9. Pressure-compression curves for gold.
See caption to Fig. 3.

to the initial energy E_{0H} can be written (since $P_{0H} \neq 0$)

$$E_H - E_{0H} = (A\mu^2 + B\mu^3 + C\mu^4) / [2\rho_0(\mu + 1)]. \quad (7)$$

Equations (5), (7), and Table II summarize all the experimental thermodynamic information which are available from the shock-wave measurements.

TABLE II. Analytical fits of Hugoniot curves, $P = A\mu + B\mu^2 + C\mu^3$, with pressure in kilobars.

| Metal | A | B | C |
|---------------|------|------|--------|
| Beryllium | 1182 | 1382 | 0 |
| Cadmium | 479 | 1087 | 2829 |
| Chromium | 2070 | 2236 | 7029 |
| Cobalt | 1954 | 3889 | 1728 |
| Copper | 1407 | 2871 | 2335 |
| Gold | 1727 | 5267 | 0 |
| Lead | 417 | 1159 | 1010 |
| Magnesium | 370 | 540 | 186 |
| Molybdenum | 2686 | 4243 | 733 |
| Nickel | 1963 | 3750 | 0 |
| Silver | 1088 | 2687 | 2520 |
| Thorium | 572 | 646 | 855 |
| Tin | 432 | 878 | 1935 |
| Titanium | 990 | 1168 | 1246 |
| Zinc | 662 | 1577 | 1242 |
| 24ST aluminum | 765 | 1659 | 428 |
| Brass | 1037 | 2177 | 3275 |
| Indium | 496 | 1163 | 0 |
| Niobium | 1658 | 2786 | 0 |
| Palladium | 1744 | 3801 | 15 230 |
| Platinum | 2760 | 7260 | 0 |
| Rhodium | 2842 | 6452 | 0 |
| Tantalum | 1790 | 3023 | 0 |
| Thallium | 317 | 938 | 1485 |
| Zirconium | 934 | 720 | 0 |

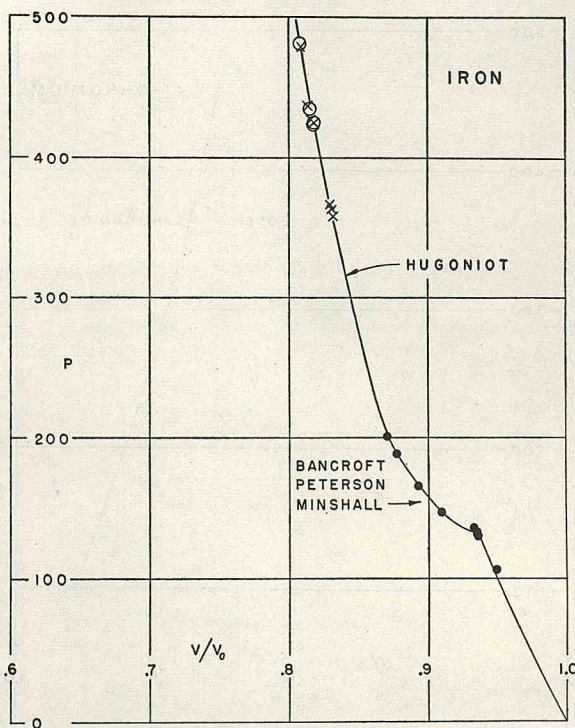


FIG. 10. Pressure-compression curves for iron.
See caption to Fig. 3.

D. Zinc Single-Crystal Experiments

Two experiments with zinc single crystals were performed to determine whether observed compressions

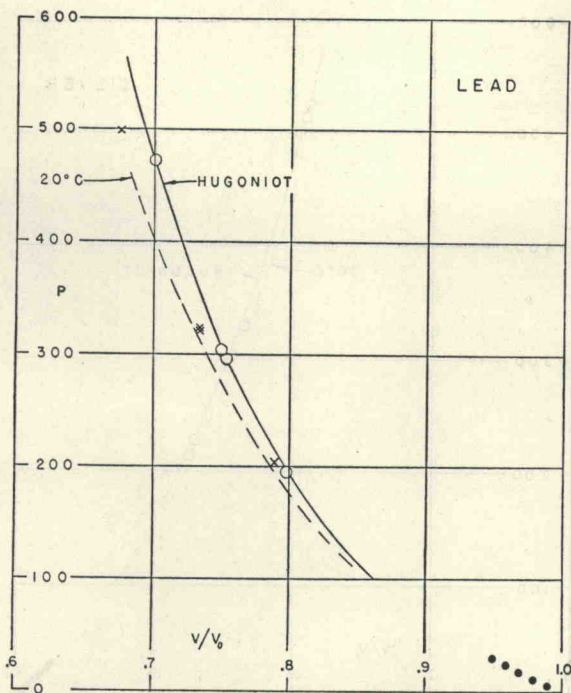


FIG. 11. Pressure-compression curves for lead.
See caption to Fig. 3.

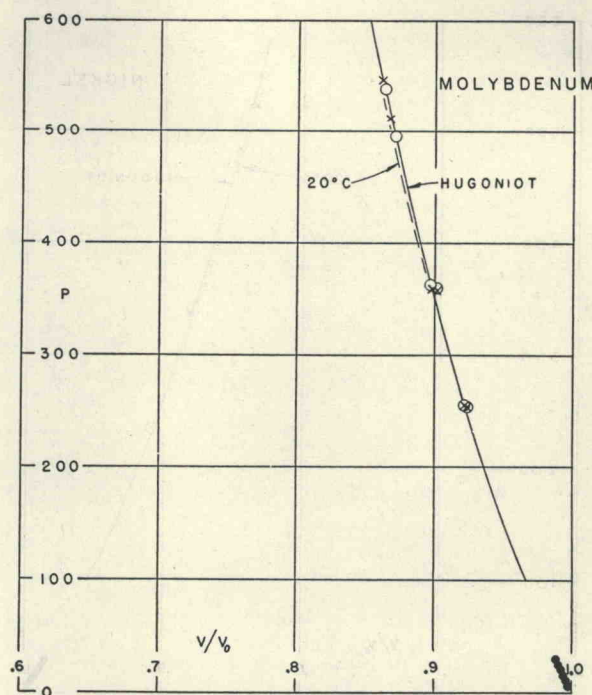


FIG. 13. Pressure-compression curves for molybdenum.
See caption to Fig. 3.

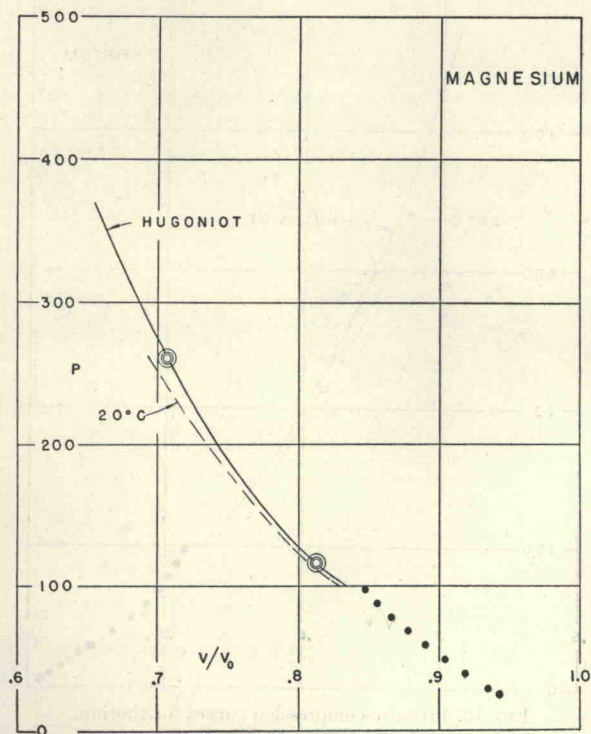


FIG. 12. Pressure-compression curves for magnesium.
See caption to Fig. 3.

were dependent upon the crystal orientation. Three zinc crystals of known orientation (shock propagation directions along the *C* axis, along an *A* axis, and midway

between two *A* axes) were used in each shot. Shock velocity was measured for each crystal and shock strength was measured for the 24ST aluminum driver plate. The measured values were then used to determine pressure-volume points by the graphical solution method.

The total spread for the three zinc shock velocities in the high-pressure (414 kilobars) shot was 1%, and the corresponding spread for the low-pressure (200 kilobars) shot was 1.5%. Comparable scatters would be expected even if identical specimens were measured so that, within experimental error, one must conclude that results show no dependence of shock velocity (hence compressibility) upon crystallographic orientation. The measured shock velocities from each shot were averaged to obtain the value used in the graphical solutions. The data are listed under zinc in Table I and are also plotted in Fig. 19, where they exhibit good agreement with results obtained using ordinary cast polycrystalline zinc.

The shock wave results differ from the lower pressure static measurements⁵ which indicate a several-fold difference in compressibility depending upon whether the compression is parallel to the *C* axis or normal to it.

E. Discussion of Experimental Data

The probable error per data point, determined from the observed reproducibility, is 0.7% in shock velocity for a given free-surface velocity (about 1% in compression, $1 - V/V_0$, at a given pressure). This estimate

⁵ P. W. Bridgman, Proc. Am. Acad. Arts Sci. 77, 189 (1949).

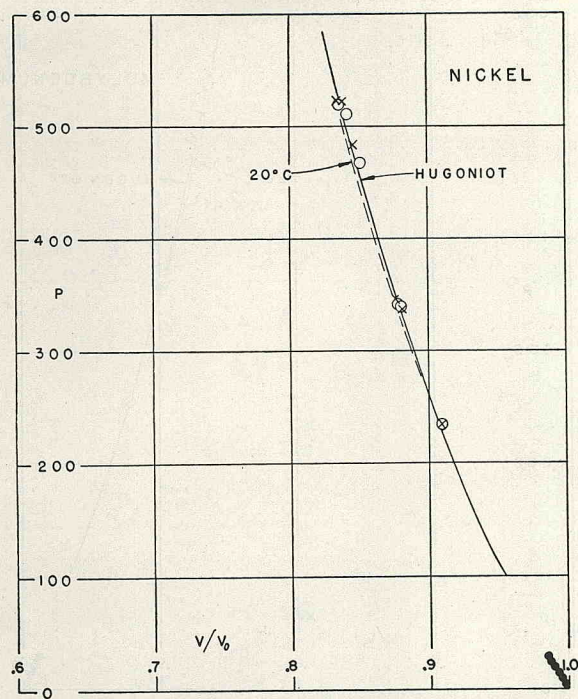


FIG. 14. Pressure-compression curves for nickel.
See caption to Fig. 3.

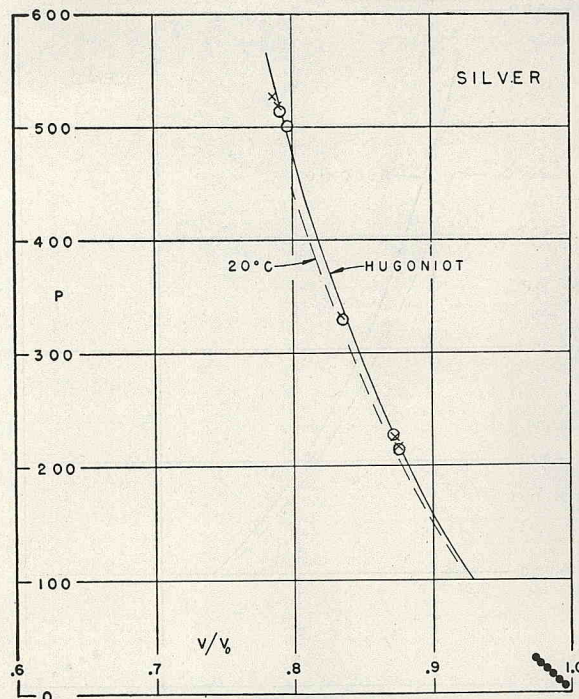


FIG. 15. Pressure-compression curves for silver.
See caption to Fig. 3.

does not apply, however, to the eight rare metals (In, Pd, Rh, Pt, Ta, Tl, Nb, Zr) at the bottom of Table I, the probable errors for which are approximately 3% in compression.

Previously reported¹ Hugoniot curves for 24ST aluminum, copper, and zinc are in substantial agreement with the present results. The present low-pressure (195-kilobar) zinc curve, however, indicates a 4% smaller compression than the previously drawn curve (Table III of reference 1). Similar comparisons of remaining data show agreement to 2% or better.

Present results may also be compared with shock-wave data obtained by another Los Alamos group using an electrical pin-contact method.² The agreement with their tabulated "recent data" (24ST aluminum data sufficient to determine the Hugoniot curve from 145 to 330 kilobars) is everywhere better than 1% in compression, and is sufficiently good to indicate freedom from sizable consistent error of either method.

Impurities for the elements studied were determined by spectrochemical analysis. Specimens whose impurities exceeded 0.2% are: cobalt (0.5% Ni, 0.05% miscellaneous), nickel (0.1% Co, 0.05% each Mg, Si, Mn, Fe), titanium (0.05% each Al, Si, Cr, Mn, Sn).

The brass composition was 60.56% Cu, 39.31% zinc. The 24ST aluminum composition was 93.0% aluminum, 4.5% copper, 1.5% magnesium, 0.6% manganese.

F. Guide to Data Figures

The points below 100 kilobars, plotted as solid black disks in Figs. 3 to 29, are statically determined pressure-

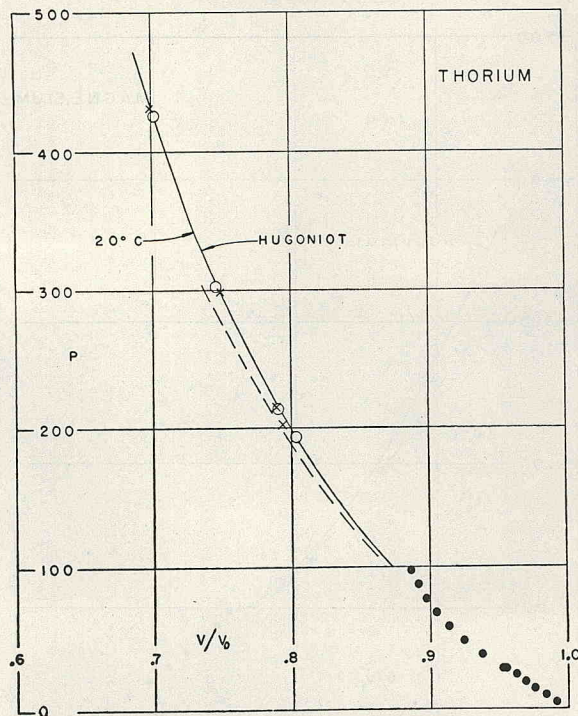


FIG. 16. Pressure-compression curves for thorium.
See caption to Fig. 3.

compression data taken from four articles by Bridgman.⁵⁻⁸

Except for the points around 400 kilobars, the iron

⁶ P. W. Bridgman, Proc. Am. Acad. Arts Sci. **76**, 55 (1948).

⁷ P. W. Bridgman, Proc. Am. Acad. Arts Sci. **76**, 9 (1945).

⁸ P. W. Bridgman, Proc. Am. Acad. Arts Sci. **74**, 425 (1945).

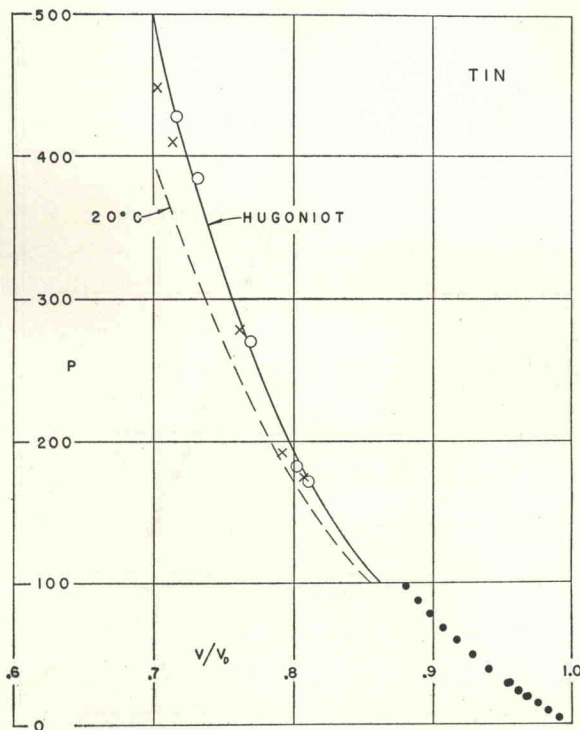


FIG. 17. Pressure-compression curves for tin.
See caption to Fig. 3.

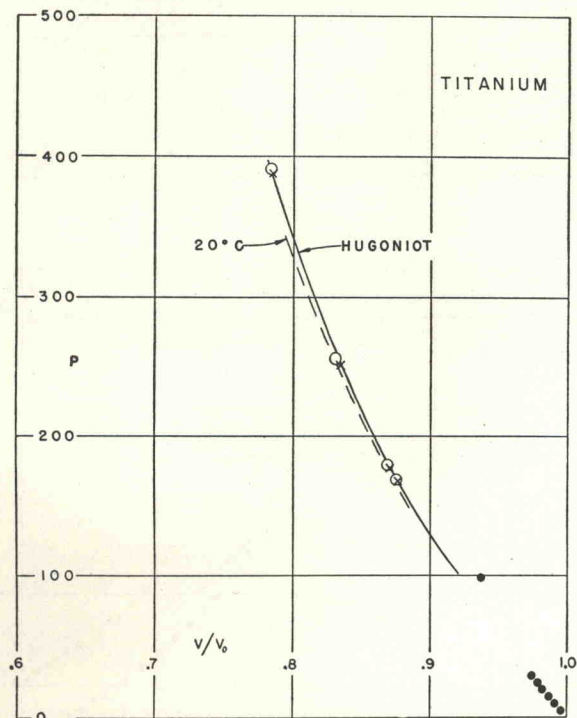


FIG. 18. Pressure-compression curves for titanium.
See caption to Fig. 3.

data of Fig. 10 are reproduced from a recent article by Bancroft, Peterson, and Minshall.⁹

⁹ Bancroft, Peterson, and Minshall, *J. Appl. Phys.* **27**, 291 (1956).

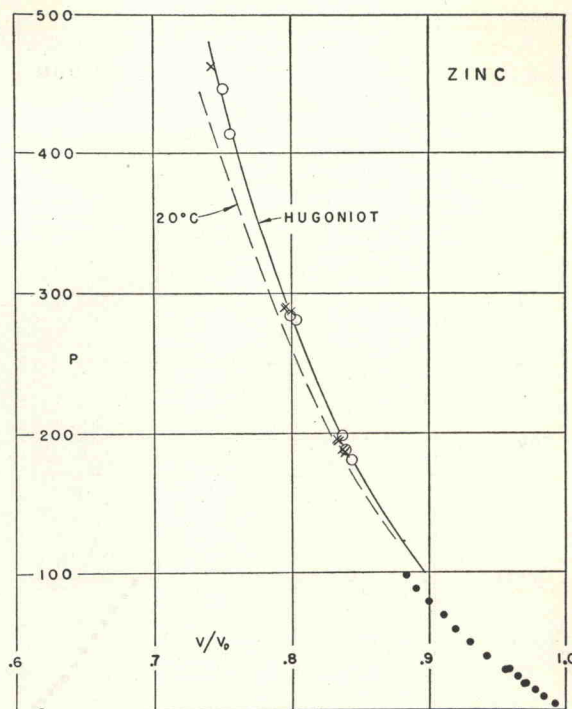


FIG. 19. Pressure-compression curves for zinc.
See caption to Fig. 3.

II. EQUATION OF STATE

The purpose of the present section is to provide a complete thermodynamic description of all states neighboring the experimental Hugoniot curves. To this end, the Mie-Grüneisen equation of state is employed, for which the volume dependence of the Grüneisen ratio is determined using the Dugdale-MacDonald relation. These considerations lead to a complete P , V , E equation of state. This equation of state and available zero-pressure data then permit the calculation of remaining thermodynamic data of interest, and numerical results are tabulated for the various metals.

A. Theory

Mie-Grüneisen Equation of State

For the thermodynamic states of interest here, we shall assume that the thermal energy of a metallic crystal can be adequately described by means of a set of simple harmonic oscillators (the normal modes of the dynamical system) whose frequencies, ν_α , are functions only of volume. The internal energy, E , is then given by¹⁰⁻¹²

$$E = \Phi + \frac{1}{2} \sum_{\alpha} h\nu_{\alpha} + \sum_{\alpha} \frac{h\nu_{\alpha}}{e^{h\nu_{\alpha}/kT} - 1}, \quad \alpha = 1, \dots, 3N, \quad (8)$$

¹⁰ See, for example, J. C. Slater, *Introduction to Chemical Physics* (McGraw-Hill Book Company, Inc., New York, 1939), Chap. XIII.

¹¹ F. Seitz, *Modern Theory of Solids* (McGraw-Hill Book Company, Inc., New York and London, 1940), Chap. III.

¹² M. Born and K. Huang, *Dynamical Theory of Crystal Lattices* (Clarendon Press, Oxford, 1954), Chap. II.

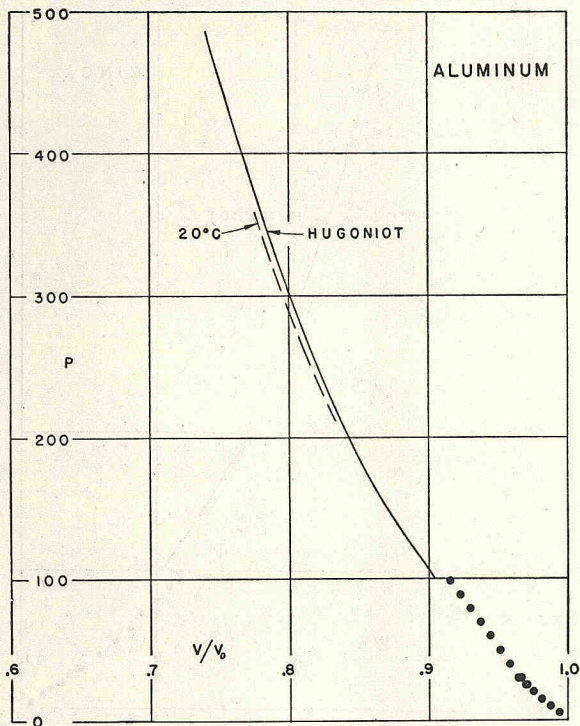


FIG. 20. Pressure-compression curves for 24ST aluminum.
See caption to Fig. 3.

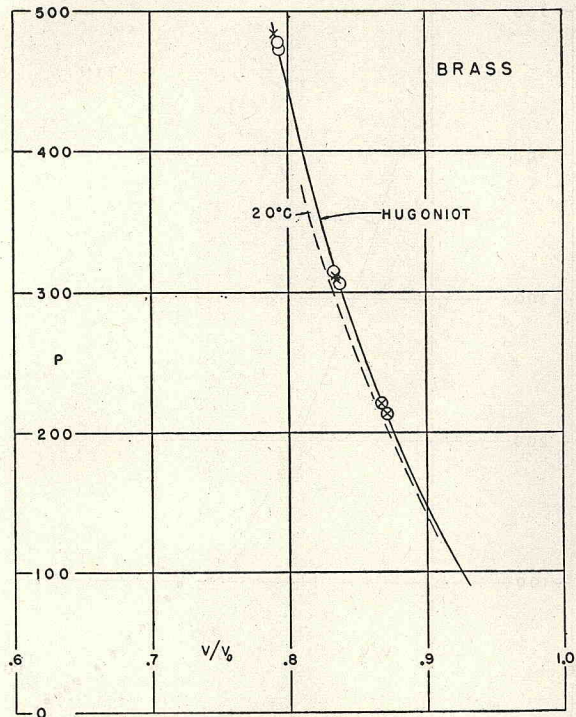


FIG. 21. Pressure-compression curves for brass.
See caption to Fig. 3.

where Φ is the potential energy of the crystal with the particles at rest in their equilibrium positions, and the summation (\sum_{α}) is over the $3N$ normal modes of the crystal, N being the total number of atoms.

The pressure is given by

$$P = -\frac{d\Phi}{dV} + \frac{1}{V} \sum \gamma_{\alpha} \left\{ \frac{1}{2} h\nu_{\alpha} + \frac{h\nu_{\alpha}}{e^{h\nu_{\alpha}/kT} - 1} \right\}, \quad (9)$$

where

$$\gamma_{\alpha} = -d \ln \nu_{\alpha} / d \ln V. \quad (10)$$

Equation (9) simplifies in two interesting cases. If all the γ_{α} are equal (the consequences of simplifying assumptions discussed below), these quantities may be factored from the summation as γ . Alternatively, in the classical limit, the energies of all oscillators are equal, so that these quantities may be factored and γ becomes the average of the γ_{α} . In either case Eq. (9) reduces to the equation of state of Mie and Grüneisen,¹³

$$P = -\frac{d\Phi}{dV} + \frac{\gamma}{V} E_{\text{vib}}, \quad (11)$$

where E_{vib} is the vibrational contribution to the internal energy. A rearrangement of the terms in Eq. (11) yields

$$P + \left\{ \frac{d\Phi}{dV} - \frac{\gamma}{V} \sum_{\alpha} \frac{1}{2} h\nu_{\alpha} \right\} = \frac{\gamma}{V} \sum_{\alpha} \frac{h\nu_{\alpha}}{e^{h\nu_{\alpha}/kT} - 1} \quad (12a)$$

¹³ E. Grüneisen, *Handbuch der Physik* (Verlag J. Springer, Berlin, 1926), Vol. 10, p. 22.

or

$$P - P_K = (\gamma/V) E_{\text{th}} = (\gamma/V) (E - E_K), \quad (12b)$$

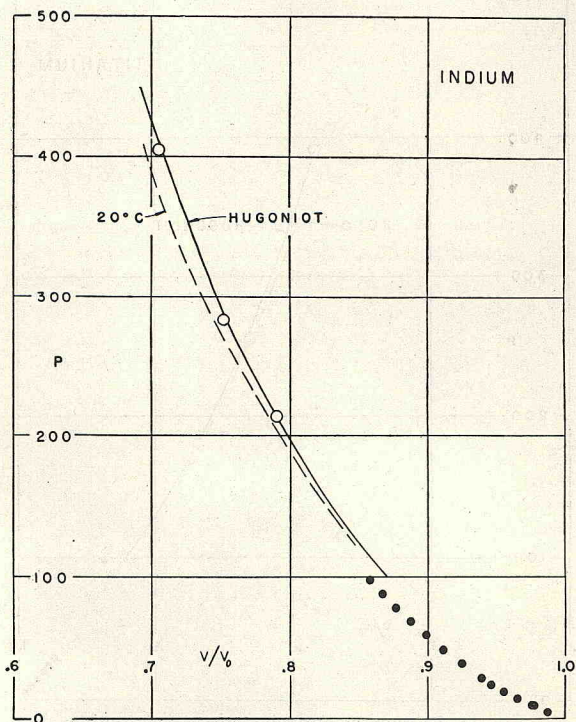


FIG. 22. Pressure-compression curves for indium.
See caption to Fig. 3.

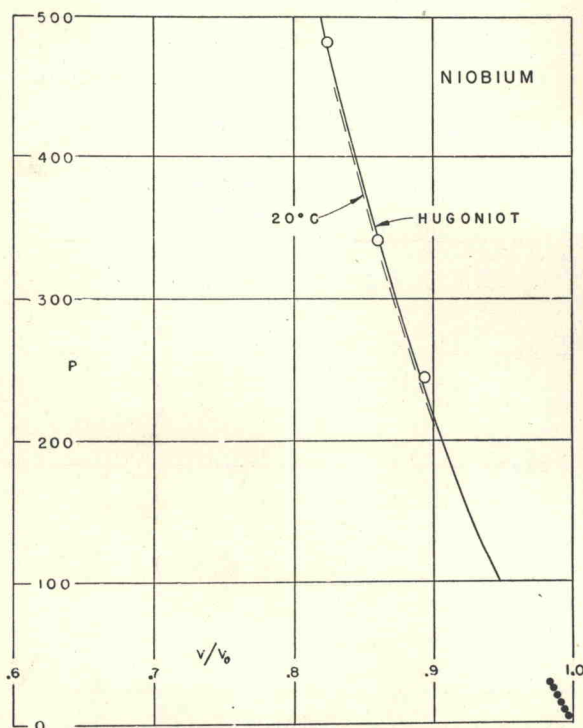


FIG. 23. Pressure-compression curves for niobium.
See caption to Fig. 3.

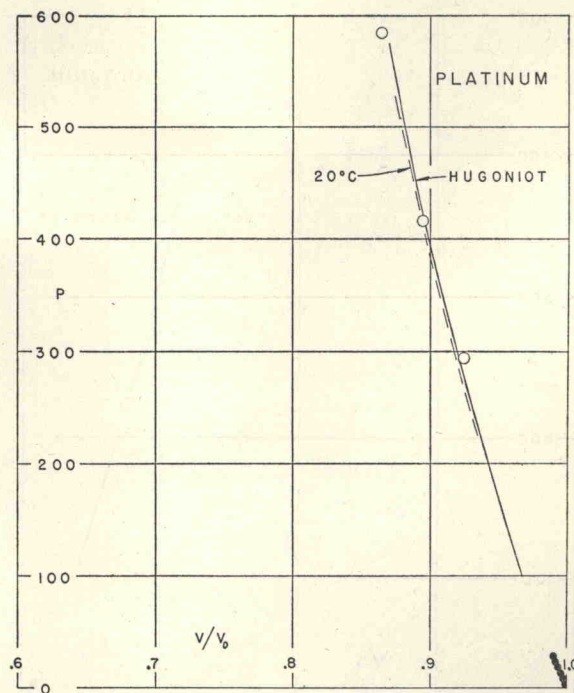


FIG. 25. Pressure-compression curves for platinum.
See caption to Fig. 3.

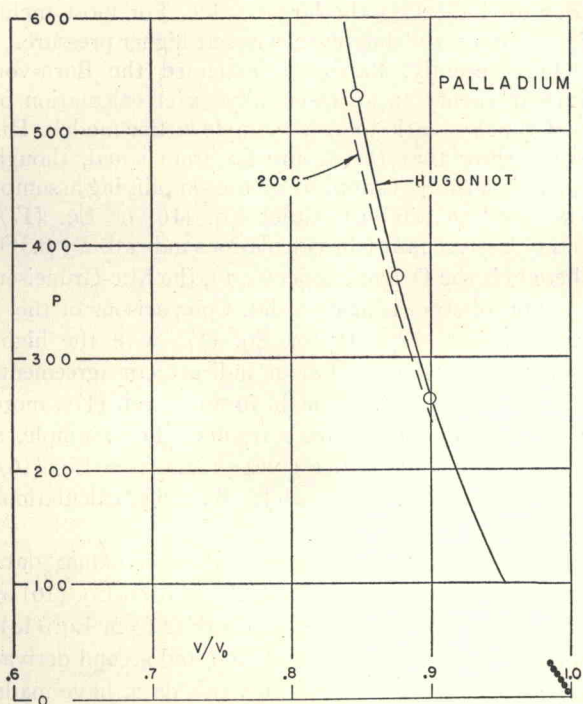


FIG. 24. Pressure-compression curves for palladium.
See caption to Fig. 3.

where the subscript K refers to the quantities as a function of volume at 0°K . Grüneisen's ratio, γ , can be

expressed in terms of thermodynamic quantities by differentiating Eq. (12b). Since γ is a function only of volume,

$$\begin{aligned}\gamma &= V \left(\frac{\partial P}{\partial E} \right)_V \equiv V \left(\frac{\partial P}{\partial T} \right)_V / C_v \\ &= -V \left(\frac{\partial P}{\partial V} \right)_T \left(\frac{\partial V}{\partial T} \right)_P / C_v \\ &= -V \left(\frac{\partial P}{\partial V} \right)_S \left(\frac{\partial V}{\partial T} \right)_P / C_p, \quad (13)\end{aligned}$$

where C_v and C_p are the specific heats at constant volume and pressure, respectively. At zero pressure and room temperature γ can be evaluated from the measured values of the bulk modulus, thermal expansion coefficient, and specific heat; and for most metals the value so obtained lies between 1 and 3 (see Table III).

Equation (12b) can be rewritten in terms of any P , V , E curve, such as the experimental Hugoniot:

$$P - P_H = (\gamma/V)(E - E_H). \quad (14)$$

Determination below of the Grüneisen ratio $\gamma(V)$ then provides one with a complete P , V , E equation of state.

It is interesting to note, with respect to C_v , that the thermodynamic identity

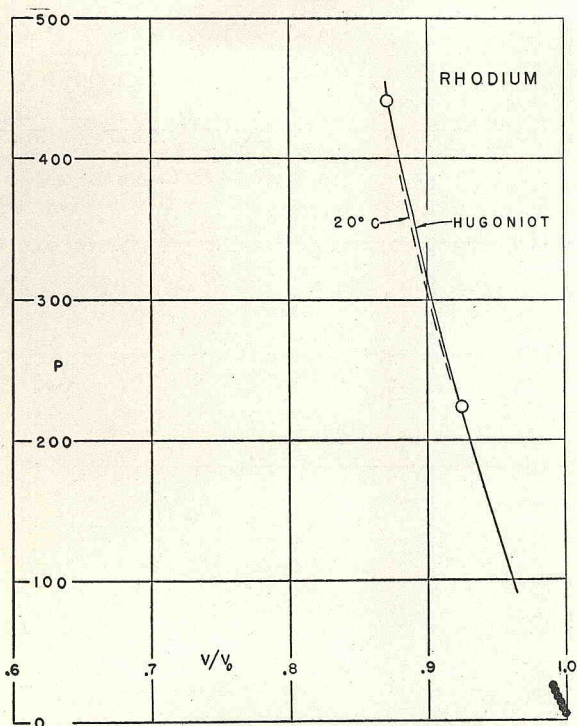


FIG. 26. Pressure-compression curves for rhodium.
See caption to Fig. 3.

$$\left(\frac{\partial C_v}{\partial T}\right)_s = \frac{C_v}{T} + T \left(\frac{\partial P}{\partial T}\right)_v \left\{ \frac{\partial}{\partial T} \left[\frac{C_v}{T(\partial P/\partial T)_v} \right] \right\}, \quad (15)$$

for γ a function only of volume, implies that C_v is a function only of entropy.

Grüneisen Ratio

Under the assumption that Poisson's ratio is independent of volume, Slater¹⁴ extended the Debye theory for an isotropic continuum to obtain

$$\gamma = -\frac{V}{2} \left(\frac{d^2 P/dV^2}{dP/dV} \right) - \frac{2}{3}. \quad (16)$$

Dugdale and MacDonald¹⁵ proposed a modification of Slater's formula. Their result,

$$\gamma = -\frac{V}{2} \left(\frac{d^2(PV^{2/3})/dV^2}{d(PV^{2/3})/dV} \right) - \frac{1}{3}, \quad (17)$$

follows for cubic lattices from the assumption that all of the interatomic force constants change the same (percentagewise) upon compression of the lattice.¹⁶

¹⁴ Reference 10, p. 239.

¹⁵ J. S. Dugdale and D. K. C. MacDonald, Phys. Rev. **89**, 832 (1953).

¹⁶ Detailed in a forthcoming article "Compression of Solids by Strong Shock Waves" by Rice, McQueen, and Walsh, to appear in *Solid State Physics, Advances in Research and Application* (Academic Press, Inc., New York, 1957), Vol. VI. Zero-pressure tests of Eq. (17), results of which are summarized above, are also presented.

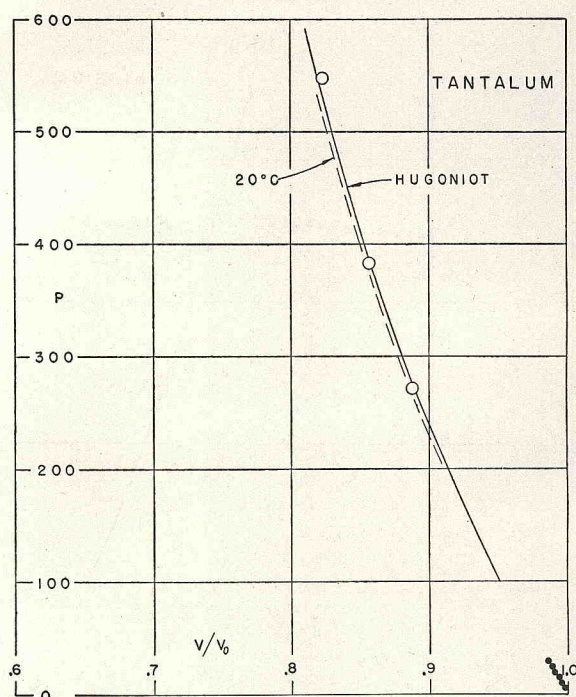


FIG. 27. Pressure-compression curves for tantalum.
See caption to Fig. 3.

Equations (16) and (17) differ by 0.33 at $P=0$, with Eq. (16) indicating the larger value. For most metal $P-V$ curves, the difference is less at higher pressure.

Quite recently, Barron^{17,18} extended the Born-von Kármán theory to an essentially exact calculation of the Grüneisen ratio for a few simple lattice models. His results show that the γ_α are far from equal, though equality of the γ_α is implied by the simplifying assumptions used to establish either Eq. (16) or Eq. (17). In the classical limit (the calculations indicate $T \gtrsim 0.3\Theta$, where Θ is the Debye temperature), the Mie-Grüneisen equation of state is again valid. Comparisons of the γ obtained from Eq. (16) or Eq. (17) with the high-temperature results by Barron indicate fair agreement, with the Dugdale-MacDonald formula, Eq. (17), more nearly reproducing Barron's results. [For example, a model of the NaCl lattice gives $\gamma=2.3$ from Eq. (16), $\gamma=2.0$ from Eq. (17), while Barron's calculations indicate $\gamma=1.67$.]

At zero pressure, sufficient thermodynamic data exist to test the values of γ calculated from Eq. (16) or (17) against the thermodynamic values from Eq. (13). Slater^{19,20} and Gilvarry,²¹ using first and second derivatives of P obtained from Bridgman's data, have made extensive comparisons of the γ calculated from Eq. (16)

¹⁷ T. H. K. Barron, Ann. Phys. **1**, 77 (1957).

¹⁸ T. H. K. Barron, Phil. Mag. **46**, 720 (1955).

¹⁹ J. C. Slater, reference 10, Chap. XXVII.

²⁰ J. C. Slater, Phys. Rev. **57**, 744 (1940).

²¹ J. J. Gilvarry, Phys. Rev. **102**, 331 (1956).

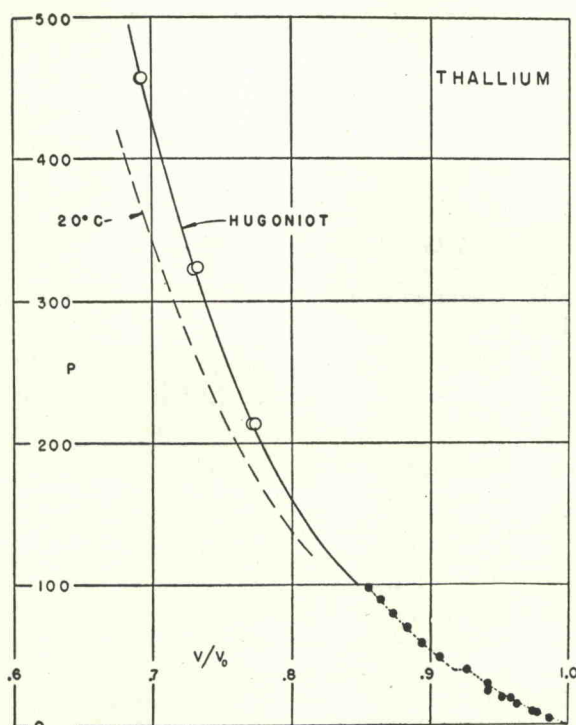


FIG. 28. Pressure-compression curves for thallium.
See caption to Fig. 3.

with that from Eq. (13). For most metals the agreement is quite good. A similar comparison, using the present shock-wave data, has been carried out by the present authors.¹⁶ Such a test is of interest because the shock wave results limit properly at zero pressure to the desired adiabatic first and second derivatives; also the extended data region of the present experimentation should lead to better precision in the determination of second derivatives of P . The tests, which show less scatter than the previous work, indicate somewhat more success for the Dugdale-MacDonald formula, Eq. (17), than for Eq. (16), though both are in substantial agreement with the experimental results. The former reproduces the values of γ from Eq. (13) with an average error of 15%.

In the following calculations, an attempt is made to obtain the most accurate description of high-pressure states. Accordingly, the experimental thermodynamic properties, i.e., of specific heats, thermal expansions, and γ_0 , are employed along the zero-pressure isobars, and only the volume variation of γ is estimated by an empirical relation. The Dugdale-MacDonald formula, Eq. (17), is employed for this purpose. It is, of course, clear that the calculated values of γ , at high pressures, are not very accurate. In regard to calculated P - V curves, on the other hand, γ is used only to estimate the small offsets (typically 1% in volume) from the experimental Hugoniot and errors as large as 25% in the offsets (i.e., approximately 25% in γ) lead to uncer-

TABLE III. Analytical fits of Grüneisen ratios.
 $\gamma = \gamma_0 + A\mu + B\mu^2 + C\mu^3$.

| Metal | γ_0 | A | B | C |
|---------------|------------|---------|---------|---------|
| Beryllium | 1.17 | -2.523 | 12.990 | -31.851 |
| Cadmium | 2.27 | 13.417 | -75.631 | 72.965 |
| Chromium | 1.08 | 10.965 | -54.874 | 49.000 |
| Cobalt | 1.99 | -5.906 | 26.354 | -48.076 |
| Copper | 2.04 | -3.296 | 10.493 | -19.264 |
| Gold | 3.05 | -21.876 | 115.18 | -213.17 |
| Lead | 2.78 | -8.406 | 22.791 | -22.648 |
| Magnesium | 1.46 | -2.078 | 4.621 | -4.840 |
| Molybdenum | 1.58 | -4.600 | 25.837 | -61.398 |
| Nickel | 1.91 | -8.007 | 35.275 | -59.812 |
| Silver | 2.47 | -5.670 | 19.334 | 32.891 |
| Thorium | 1.124 | 3.552 | -14.223 | 15.552 |
| Tin | 2.03 | 9.4186 | -52.133 | 66.016 |
| Titanium | 1.18 | 2.225 | -9.904 | 11.052 |
| Zinc | 2.38 | -6.087 | 18.626 | -23.535 |
| 24ST aluminum | 2.13 | -7.245 | 24.707 | -32.577 |
| Brass | 2.04 | 3.405 | -26.304 | 38.692 |
| Indium | 2.238 | -9.431 | 27.392 | -26.186 |
| Niobium | 1.679 | -5.882 | 26.261 | -49.145 |
| Palladium | 2.183 | 26.824 | -205.44 | 407.72 |
| Platinum | 2.627 | -16.911 | 100.10 | -216.84 |
| Rhodium | 2.265 | -11.228 | 55.898 | -109.85 |
| Tantalum | 1.689 | -5.166 | 15.925 | -18.991 |
| Thallium | 2.96 | -3.617 | 2.264 | -1.171 |
| Zirconium | 0.771 | -0.449 | 0.285 | -0.102 |

tainties which are only comparable to probable errors in the experimental curves. Temperature increases, calculated along constant-entropy curves, reflect an error which is roughly proportional to the volume-average error in γ . The use of the correct γ_0 at normal

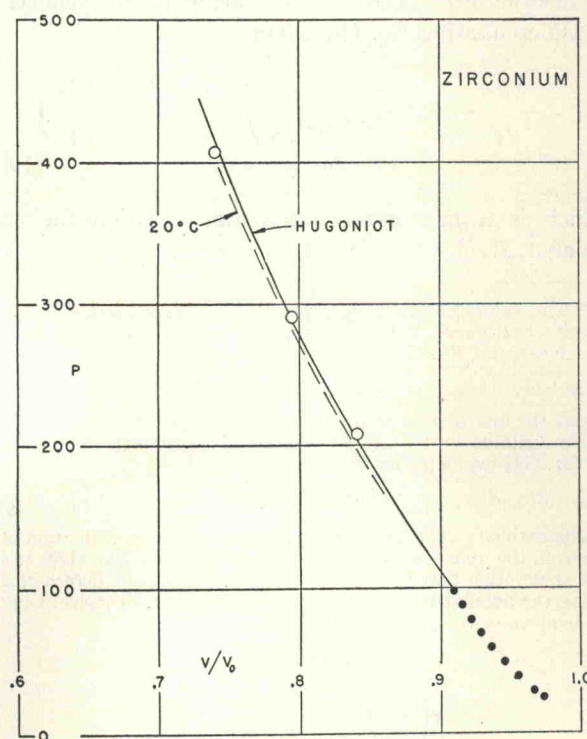


FIG. 29. Pressure-compression curves for zirconium.
See caption to Fig. 3.

volume and an experimental additive term in the listed temperatures (T at $P=0$ on the adiabat through the point) then lead to temperatures which should be reliable to 10% or less of their centigrade values.

B. Calculations

Combining Eq. (17), which is assumed to be valid along the 0°K curve, with Eq. (14) yields the following equation for the pressure $P_K(V)$ at 0°K , in terms of the known Hugoniot curve, $P_H(V)$:

$$\frac{-\frac{1}{2}Vd^2(P_KV^{\frac{2}{3}})/dV^2}{d(P_KV^{\frac{2}{3}})/dV} = \frac{1}{3} \quad (18)$$

$$= \frac{V(P_H - P_K)}{\frac{1}{2}P_H(V_{0H} - V) + E_{0H} + \int_{V_{0K}}^V PdV}$$

The initial conditions required for the integration of Eq. (18) are the specific volume, the compressibility at 0°K , $P_K=0$, and the specific internal energy, E_{0H} , at the foot of the Hugoniot (relative to an arbitrary zero energy at $P=0$, $T=0^\circ\text{K}$). These quantities were obtained from rough extrapolations²² of available zero pressure data to 0°K . Zero-degree-Kelvin pressure-volume curves, obtained by numerical integration of Eq. (18), are listed in Table IV. Analytical fits of the associated $\gamma(V)$ curves, which may now be obtained from either Eq. (14) or Eq. (17), are given in Table III.

Differentiating Eq. (14) gives

$$P_A = -\frac{dE_H}{dV} + (P_H - P_A)\frac{d}{dV}\left(\frac{V}{\gamma}\right) + \frac{V}{\gamma}\left(\frac{dP_H}{dV} - \frac{dP_A}{dV}\right), \quad (19)$$

which is a first order differential equation for an adiabat, $P_A(V)$, in terms of the known $P_H(V)$, $E_H(V)$,

²² The values of E_{0H} were obtained by integrating the Debye specific heat curve. Values of the initial volume, V_{0K} , were those which satisfied Eq. (14) evaluated at $V=V_{0K}$:

$[\gamma_{0H} + (d\gamma/dV)_{0H}(V_{0H} - V_{0K})][E_{0H} + \frac{1}{2}P_H(V_{0H} - V_{0K})] = V_{0K}P_H$, where the first bracket is an approximate value for γ at V_{0K} . The compressibility at 0°K , $P_K=0$, was obtained from the derivative of Eq. (14) evaluated at $V=V_{0K}$:

$$V_{0K}(dP_K/dV)_{V=V_{0K}} = [P_H - E_H(d\gamma/dV) - \gamma(dE_H/dV)]_{V=V_{0K}}$$

Approximate values of $d\gamma/dV$, necessary for the evaluation of each of the above relations, were obtained from Eq. (17), and the assumption that the right side of Eq. (17) can be determined using the adiabat through the foot of the Hugoniot curve. Consequent values of γ_0 and $d\gamma/dV$ are

$$\gamma_{0H} = B/A,$$

$$V_{0H}\left(\frac{d\gamma}{dV}\right)_{0H} = \frac{5B^2}{2A^2} - \frac{7B}{6A} - \frac{C}{A} - \frac{1}{9}$$

The first of these relations was also used in Sec. I to determine the values of B/A used in analytical fits of the experimental data.

and $\gamma(V)$. Equation (19) was integrated numerically to obtain several adiabats for each metal. Two of these, the adiabat which coincides with the foot of the Hugoniot and an adiabat which intersects the Hugoniot curve at a pressure near the upper limit of the experimental data, are listed in Table IV.

At constant entropy the thermodynamic identity

$$TdS = C_v dT + T(\partial P/\partial T)_V dV = 0$$

can be integrated to give temperature as a function of volume:

$$T = T_i \exp\left[-\int_{V_i}^V \frac{\gamma}{V} dV\right]. \quad (20)$$

Here the relation $\gamma = V(\partial P/\partial T)_V/C_v$ was used, and T_i is an initial temperature at some volume V_i on the adiabat. Values of T_i , V_i were obtained along $P=0$ from available thermal expansion data. Equation (20) can then be used together with the adiabatic P - V curves determined above to obtain the temperature at any P - V point neighboring the Hugoniot curve. Resulting temperatures for pressure-volume points along two adiabats are listed in Table IV. Temperatures along the Hugoniot curve for each metal are also listed in Table IV and the 20°C isotherms are plotted in Figs. 3-29.

Calculated values of the ratio

$$\frac{U_r}{U_p} = \int_0^{P_H} (-dV/dP_A)^{\frac{1}{2}} dP_A / [P_H(V_{0H} - V)]^{\frac{1}{2}} \quad (21)$$

(see Eq. 4 and associated discussion) are listed in Table V for the various solids. The denominator in Eq. (21) is the expression for the shock wave particle velocity corresponding to shock pressure P_H and is a consequence of Eqs. (1) and (2). The numerator²³ is the Reimann integral for the particle velocity due to the centered, simple rarefaction wave which relieves the pressure from P_H to zero, and is evaluated using the adiabat which intersects the Hugoniot curve at P_H . The refinements indicated by the present calculations cause a slight shift of the P , V points, plotted as \times 's in the figures, which were obtained by using Eq. (4). The corrections reduce the compression offsets (between the \times 's and the curves drawn through the graphical solutions) from an average magnitude of 1.1% to 0.7%.

It should be noted that three metals, lead, tin and cadmium, exhibit free-surface-approximation solutions which are in sizable disagreement with results obtained from the graphical solutions. The three are all low-melting-point metals and are, indeed, the only metals (among those for which free-surface velocity measure-

²³ See, for example, R. Courant and K. O. Friedrichs, *Supersonic Flow and Shock Waves* (Interscience Publishers, Inc., New York, 1948). The present expression can be obtained from their Eq. (34.05).

TABLE IV. Pressure-volume loci and associated temperatures (degrees centigrade). The first adiabat listed for each material coincides with the Hugoniot curve at 20°C, zero pressure. The second adiabat intersects the Hugoniot curve near the high-pressure limit of the experimental data. The pressure at which the second adiabat crosses the Hugoniot curve is given in parentheses.

| $\backslash P$ (kilobars) | 0 | 100 | 150 | 200 | 250 | 300 | 350 | 400 | 450 | 500 |
|---------------------------|--------|--------|--------|--------|--------|--------|--------|--------|--------|--------|
| Beryllium | | | | | | | | | | |
| 0°K | 0.9982 | 0.9263 | 0.8972 | 0.8716 | 0.8487 | 0.8275 | 0.8082 | | | |
| Hugoniot | 1.000 | 0.9277 | 0.8990 | 0.8725 | 0.8503 | 0.8299 | 0.8110 | | | |
| T_H | 20°C | 50° | 70° | 97° | 127° | 168° | 213° | | | |
| Adiabat | 1.000 | 0.9276 | 0.8987 | 0.8728 | 0.8493 | 0.8284 | | | | |
| T_A | 20°C | 45 | 55 | 64 | 74 | 82 | | | | |
| Adiabat (309 kilobars) | 1.003 | 0.9301 | 0.9010 | 0.8742 | 0.8506 | 0.8299 | 0.8103 | | | |
| T_A | 97°C | 129 | 143 | 155 | 164 | 181 | 187 | | | |
| Cadmium | | | | | | | | | | |
| 0°K | 0.9764 | 0.8524 | 0.8188 | 0.7932 | 0.7716 | 0.7527 | 0.7364 | 0.7220 | 0.7093 | 0.6972 |
| Hugoniot | 1.000 | 0.8742 | 0.8403 | 0.8141 | 0.7932 | 0.7752 | 0.7597 | 0.7464 | 0.7345 | 0.7237 |
| T_H | 20°C | 210 | 349 | 515 | 697 | 895 | 1111 | 1335 | 1563 | 1800 |
| Adiabat | 1.000 | 0.8708 | 0.8339 | 0.8050 | 0.7819 | 0.7620 | 0.7450 | 0.7300 | 0.7164 | 0.7041 |
| T_A | 20°C | 157 | 213 | 257 | 297 | 331 | 359 | 384 | 408 | 431 |
| Adiabat (318 kilobars) | 1.028 | 0.8976 | 0.8568 | 0.8244 | 0.7982 | 0.7763 | 0.7573 | 0.7414 | 0.7265 | 0.7136 |
| T_A | 310°C | 559 | 674 | 784 | 866 | 945 | 1014 | 1072 | 1125 | 1177 |
| Chromium | | | | | | | | | | |
| 0°K | 0.9969 | 0.9528 | 0.9336 | 0.9160 | 0.9006 | 0.8860 | 0.8730 | 0.8607 | 0.8492 | 0.8387 |
| Hugoniot | 1.000 | 0.9561 | 0.9373 | 0.9202 | 0.9050 | 0.8908 | 0.8779 | 0.8658 | 0.8548 | 0.8447 |
| T_H | 20°C | 39 | 54 | 73 | 96 | 126 | 161 | 199 | 242 | 291 |
| Adiabat | 1.000 | 0.9561 | 0.9372 | 0.9201 | 0.9044 | 0.8899 | 0.8717 | 0.8642 | 0.8529 | 0.8421 |
| T_A | 20°C | 37 | 46 | 56 | 66 | 76 | 86 | 95 | 103 | 112 |
| Adiabat (522 kilobars) | 1.003 | 0.9595 | 0.9410 | 0.9238 | 0.9081 | 0.8933 | 0.8798 | 0.8674 | 0.8560 | 0.8449 |
| T_A | 170°C | 194 | 209 | 223 | 238 | 253 | 267 | 281 | 295 | 307 |
| Cobalt | | | | | | | | | | |
| 0°K | 0.9931 | 0.9500 | 0.9318 | 0.9150 | 0.9000 | 0.8863 | 0.8734 | 0.8612 | 0.8500 | 0.8395 |
| Hugoniot | 1.000 | 0.9552 | 0.9368 | 0.9200 | 0.9050 | 0.8915 | 0.8782 | 0.8660 | 0.8551 | 0.8450 |
| T_H | 20°C | 48 | 65 | 86 | 109 | 134 | 166 | 202 | 241 | 283 |
| Adiabat | 1.000 | 0.9552 | 0.9366 | 0.9197 | 0.9045 | 0.8905 | 0.8770 | 0.8645 | 0.8531 | 0.8422 |
| T_A | 20°C | 45 | 57 | 67 | 76 | 86 | 96 | 104 | 111 | 117 |
| Adiabat (523 kilobars) | 1.005 | 0.9581 | 0.9392 | 0.9221 | 0.9065 | 0.8926 | 0.8792 | 0.8674 | 0.8551 | 0.8447 |
| T_A | 120°C | 155 | 171 | 185 | 199 | 211 | 224 | 235 | 245 | 254 |
| Copper | | | | | | | | | | |
| 0°K | 0.9903 | 0.9337 | 0.9109 | 0.8908 | 0.8732 | 0.8571 | 0.8424 | 0.8290 | 0.8165 | 0.8049 |
| Hugoniot | 1.000 | 0.9412 | 0.9186 | 0.8980 | 0.8803 | 0.8643 | 0.8500 | 0.8370 | 0.8249 | 0.8137 |
| T_H | 20°C | 63 | 89 | 121 | 158 | 201 | 255 | 311 | 373 | 444 |
| Adiabat | 1.000 | 0.9408 | 0.9180 | 0.8974 | 0.8781 | 0.8625 | 0.8472 | 0.8334 | 0.8209 | 0.8092 |
| T_A | 20°C | 57 | 73 | 85 | 99 | 111 | 123 | 134 | 145 | 155 |
| Adiabat (504 kilobars) | 1.010 | 0.9490 | 0.9255 | 0.9038 | 0.8852 | 0.8683 | 0.8528 | 0.8387 | 0.8255 | 0.8143 |
| T_A | 215°C | 279 | 306 | 331 | 353 | 375 | 395 | 415 | 432 | 448 |
| Gold | | | | | | | | | | |
| 0°K | 0.9900 | 0.9458 | 0.9277 | 0.9113 | 0.8966 | 0.8829 | 0.8707 | 0.8589 | 0.8480 | 0.8377 |
| Hugoniot | 1.000 | 0.9521 | 0.9334 | 0.9167 | 0.9018 | 0.8882 | 0.8759 | 0.8643 | 0.8537 | 0.8438 |
| T_H | 20°C | 65 | 96 | 121 | 153 | 200 | 253 | 311 | 372 | 443 |
| Adiabat | 1.000 | 0.9520 | 0.9331 | 0.9161 | 0.9014 | 0.8874 | 0.8744 | 0.8626 | 0.8514 | 0.8412 |
| T_A | 20°C | 59 | 74 | 86 | 97 | 108 | 117 | 125 | 133 | 141 |
| Adiabat (518 kilobars) | 1.009 | 0.9583 | 0.9382 | 0.9210 | 0.9053 | 0.8910 | 0.8779 | 0.8660 | 0.8546 | 0.8441 |
| T_A | 235°C | 311 | 338 | 361 | 383 | 401 | 419 | 434 | 449 | 464 |
| Lead | | | | | | | | | | |
| 0°K | 0.9762 | 0.8492 | 0.8113 | 0.7808 | 0.7558 | 0.7340 | 0.7150 | 0.6979 | 0.6829 | 0.6690 |
| Hugoniot | 1.000 | 0.8623 | 0.8253 | 0.7958 | 0.7722 | 0.7523 | 0.7348 | 0.7191 | 0.7051 | 0.6930 |
| T_H | 20°C | 228 | 375 | 609 | 861 | 1150 | 1459 | 1812 | 2192 | 2575 |
| Adiabat | 1.000 | 0.8600 | 0.8203 | 0.7888 | 0.7628 | 0.7403 | 0.7206 | 0.7034 | 0.6878 | 0.6736 |
| T_A | 20°C | 139 | 179 | 210 | 241 | 267 | 289 | 310 | 329 | 360 |
| Adiabat (204 kilobars) | 1.020 | 0.8695 | 0.8288 | 0.7959 | 0.7696 | 0.7465 | 0.7266 | 0.7585 | 0.7426 | 0.7280 |
| T_A | 249°C | 485 | 563 | 624 | 682 | 730 | 773 | 814 | 854 | 891 |

TABLE IV.—Continued.

| $\backslash P$ (kilobars) | 0 | 100 | 150 | 200 | 250 | 300 | 350 | 400 | 450 | 500 |
|---------------------------|--------|--------|--------|--------|--------|--------|--------|--------|--------|--------|
| Magnesium | | | | | | | | | | |
| 0°K | 0.9985 | 0.8200 | 0.7604 | 0.7304 | 0.6980 | 0.6699 | | | | |
| Hugoniot | 1.000 | 0.8300 | 0.7712 | 0.7432 | 0.7123 | 0.6861 | | | | |
| T_H | 20°C | 174 | 313 | 487 | 691 | 923 | | | | |
| Adiabat | 1.000 | 0.8278 | 0.7670 | 0.7362 | 0.7032 | 0.6737 | | | | |
| T_A | 20°C | 74 | 131 | 155 | 176 | 196 | | | | |
| Adiabat (229 kilobars) | 1.023 | 0.8395 | 0.7769 | 0.7450 | 0.7110 | 0.6816 | | | | |
| T_A | 296°C | 447 | 526 | 576 | 620 | 660 | | | | |
| Molybdenum | | | | | | | | | | |
| 0°K | 0.9971 | 0.9636 | 0.9486 | 0.9347 | 0.9219 | 0.9096 | 0.8979 | 0.8870 | 0.8768 | 0.8670 |
| Hugoniot | 1.000 | 0.9660 | 0.9510 | 0.9369 | 0.9240 | 0.9119 | 0.9002 | 0.8895 | 0.8794 | 0.8698 |
| T_H | 20°C | 37 | 49 | 62 | 79 | 101 | 125 | 154 | 188 | 227 |
| Adiabat | 1.000 | 0.9659 | 0.9508 | 0.9368 | 0.9239 | 0.9117 | 0.8999 | 0.8890 | 0.8786 | 0.8685 |
| T_A | 20°C | 35 | 43 | 49 | 55 | 61 | 67 | 72 | 77 | 83 |
| Adiabat (500 kilobars) | 1.002 | 0.9674 | 0.9522 | 0.9382 | 0.9250 | 0.9128 | 0.9011 | 0.8900 | 0.8799 | 0.8696 |
| T_A | 139°C | 161 | 171 | 180 | 189 | 197 | 205 | 213 | 221 | 228 |
| Nickel | | | | | | | | | | |
| 0°K | 0.9930 | 0.9551 | 0.9320 | 0.9151 | 0.8999 | 0.8855 | 0.8720 | 0.8599 | 0.8480 | 0.8370 |
| Hugoniot | 1.000 | 0.9501 | 0.9367 | 0.9197 | 0.9042 | 0.8900 | 0.8769 | 0.8643 | 0.8530 | 0.8422 |
| T_H | 20°C | 43 | 61 | 79 | 101 | 125 | 150 | 181 | 217 | 254 |
| Adiabat | 1.000 | 0.9500 | 0.9364 | 0.9195 | 0.9038 | 0.8890 | 0.8758 | 0.8633 | 0.8517 | 0.8401 |
| T_A | 20°C | 43 | 54 | 63 | 71 | 79 | 86 | 93 | 100 | 106 |
| Adiabat (508 kilobars) | 1.005 | 0.9588 | 0.9397 | 0.9220 | 0.9062 | 0.8918 | 0.8781 | 0.8653 | 0.8536 | 0.8423 |
| T_A | 136°C | 171 | 186 | 199 | 210 | 221 | 231 | 241 | 251 | 259 |
| Silver | | | | | | | | | | |
| 0°K | 0.9878 | 0.9202 | 0.8951 | 0.8734 | 0.8547 | 0.8380 | 0.8229 | 0.8090 | 0.7960 | 0.7833 |
| Hugoniot | 1.000 | 0.9291 | 0.9037 | 0.8818 | 0.8632 | 0.8470 | 0.8322 | 0.8190 | 0.8066 | 0.7953 |
| T_H | 20°C | 88 | 130 | 186 | 255 | 326 | 417 | 520 | 627 | 747 |
| Adiabat | 1.000 | 0.9286 | 0.9028 | 0.8804 | 0.8612 | 0.8437 | 0.8279 | 0.8138 | 0.8006 | 0.7886 |
| T_A | 20°C | 74 | 96 | 114 | 131 | 148 | 168 | 176 | 189 | 201 |
| Adiabat (479 kilobars) | 1.017 | 0.9406 | 0.9133 | 0.8900 | 0.8697 | 0.8520 | 0.8353 | 0.8207 | 0.8074 | 0.7980 |
| T_A | 314°C | 433 | 483 | 524 | 560 | 594 | 627 | 656 | 682 | 708 |
| Thorium | | | | | | | | | | |
| 0°K | 0.9920 | 0.8643 | 0.8222 | 0.7878 | 0.7594 | 0.7348 | 0.7128 | 0.6939 | 0.6767 | 0.6610 |
| Hugoniot | 1.000 | 0.8727 | 0.8310 | 0.7979 | 0.7705 | 0.7473 | 0.7274 | 0.7099 | 0.6943 | 0.6806 |
| T_H | 20°C | 122 | 227 | 377 | 552 | 752 | 969 | 1197 | 1419 | 1631 |
| Adiabat | 1.000 | 0.8716 | 0.8283 | 0.7938 | 0.7647 | 0.7396 | 0.7176 | 0.6979 | 0.6802 | 0.6634 |
| T_A | 20°C | 76 | 101 | 124 | 145 | 164 | 181 | 197 | 212 | 225 |
| Adiabat (483 kilobars) | 1.035 | 0.8989 | 0.8540 | 0.8163 | 0.7856 | 0.7586 | 0.7352 | 0.7146 | 0.6960 | 0.6784 |
| T_A | 802°C | 1003 | 1095 | 1183 | 1263 | 1339 | 1405 | 1467 | 1525 | 1581 |
| Tin | | | | | | | | | | |
| 0°K | 0.9806 | 0.8439 | 0.8068 | 0.7778 | 0.7540 | 0.7334 | 0.7159 | 0.7002 | | |
| Hugoniot | 1.000 | 0.8614 | 0.8248 | 0.7964 | 0.7735 | 0.7544 | 0.7382 | 0.7240 | | |
| T_H | 20°C | 219 | 377 | 556 | 752 | 953 | 1139 | 1318 | | |
| Adiabat | 1.000 | 0.8580 | 0.8183 | 0.7877 | 0.7622 | 0.7414 | 0.7229 | 0.7062 | | |
| T_A | 20°C | 149 | 198 | 239 | 275 | 305 | 332 | 358 | | |
| Adiabat (205 kilobars) | 1.012 | 0.8710 | 0.8297 | 0.7970 | 0.7703 | 0.7479 | 0.7289 | 0.7120 | | |
| T_A | 208°C | 415 | 497 | 569 | 631 | 683 | 731 | 773 | | |
| Titanium | | | | | | | | | | |
| 0°K | 0.9944 | 0.9119 | 0.8801 | 0.8527 | 0.8290 | 0.8077 | 0.7888 | 0.7713 | | |
| Hugoniot | 1.000 | 0.9170 | 0.8857 | 0.8587 | 0.8354 | 0.8148 | 0.7964 | 0.7809 | | |
| T_H | 20°C | 65 | 105 | 155 | 223 | 302 | 394 | 491 | | |
| Adiabat | 1.000 | 0.9168 | 0.8851 | 0.8576 | 0.8334 | 0.8118 | 0.7921 | 0.7730 | | |
| T_A | 20°C | 54 | 70 | 84 | 97 | 111 | 123 | 135 | | |
| Adiabat (340 kilobars) | 1.005 | 0.7222 | 0.8898 | 0.8618 | 0.8375 | 0.8155 | 0.7963 | 0.7776 | | |
| T_A | 210°C | 266 | 290 | 314 | 337 | 359 | 380 | 400 | | |

TABLE IV.—Continued.

| $\backslash P$ (kilobars) | 0 | 100 | 150 | 200 | 250 | 300 | 350 | 400 | 450 | 500 |
|---------------------------|--------|--------|--------|--------|--------|--------|--------|--------|--------|--------|
| Zinc | | | | | | | | | | |
| 0°K | 0.9800 | 0.8834 | 0.8507 | 0.8234 | 0.8004 | 0.7802 | 0.7622 | 0.7458 | 0.7310 | 0.7180 |
| Hugoniot | 1.000 | 0.8960 | 0.8633 | 0.8363 | 0.8140 | 0.7942 | 0.7767 | 0.7615 | 0.7482 | 0.7360 |
| T_H | 20°C | 119 | 187 | 272 | 369 | 482 | 609 | 747 | 900 | 1061 |
| Adiabat | 1.000 | 0.8949 | 0.8608 | 0.8328 | 0.8082 | 0.7875 | 0.7690 | 0.7522 | 0.7371 | 0.7232 |
| T_A | 20°C | 96 | 123 | 147 | 169 | 189 | 207 | 224 | 239 | 254 |
| Adiabat (404 kilobars) | 1.030 | 0.9126 | 0.8760 | 0.8456 | 0.8208 | 0.7985 | 0.7792 | 0.7619 | 0.7460 | 0.7318 |
| T_A | 302°C | 479 | 540 | 593 | 641 | 681 | 720 | 756 | 791 | 821 |
| Aluminum | | | | | | | | | | |
| 0°K | 0.9874 | 0.8966 | 0.8641 | 0.8362 | 0.8126 | 0.7915 | 0.7724 | 0.7553 | 0.7400 | 0.7255 |
| Hugoniot | 1.000 | 0.9045 | 0.8716 | 0.8441 | 0.8210 | 0.8008 | 0.7824 | 0.7661 | 0.7513 | 0.7380 |
| T_H | 20°C | 94 | 153 | 223 | 308 | 405 | 518 | 637 | 770 | 909 |
| Adiabat | 1.000 | 0.9036 | 0.8701 | 0.8422 | 0.8180 | 0.7961 | 0.7770 | 0.7594 | 0.7435 | 0.7288 |
| T_A | 20°C | 78 | 100 | 119 | 135 | 150 | 163 | 177 | 189 | 201 |
| Adiabat (513 kilobars) | 1.034 | 0.9250 | 0.8886 | 0.8578 | 0.8319 | 0.8092 | 0.7892 | 0.7710 | 0.7543 | 0.7392 |
| T_A | 454°C | 633 | 703 | 755 | 799 | 841 | 881 | 915 | 949 | 981 |
| Brass | | | | | | | | | | |
| 0°K | 0.9869 | 0.9140 | 0.8876 | 0.8649 | 0.8453 | 0.8283 | 0.8130 | 0.7990 | 0.7864 | 0.7745 |
| Hugoniot | 1.000 | 0.9250 | 0.8984 | 0.8758 | 0.8564 | 0.8395 | 0.8250 | 0.8115 | 0.7992 | 0.7882 |
| T_H | 20°C | 89 | 129 | 175 | 235 | 305 | 382 | 467 | 557 | 651 |
| Adiabat | 1.000 | 0.9244 | 0.8971 | 0.8739 | 0.8538 | 0.8360 | 0.8200 | 0.8056 | 0.7922 | 0.7803 |
| T_A | 20°C | 73 | 96 | 118 | 137 | 155 | 171 | 187 | 201 | 215 |
| Adiabat (446 kilobars) | 1.014 | 0.9363 | 0.9081 | 0.8839 | 0.8620 | 0.8442 | 0.8277 | 0.8129 | 0.7991 | 0.7860 |
| T_A | 230°C | 323 | 363 | 401 | 436 | 468 | 499 | 527 | 552 | 577 |
| Indium | | | | | | | | | | |
| 0°K | 0.9801 | 0.8604 | 0.8210 | 0.7880 | 0.7600 | 0.7351 | 0.7135 | 0.6943 | 0.6769 | 0.6610 |
| Hugoniot | 1.000 | 0.8701 | 0.8302 | 0.7979 | 0.7710 | 0.7478 | 0.7270 | 0.7087 | 0.6922 | 0.6774 |
| T_H | 20°C | 153 | 260 | 397 | 561 | 745 | 950 | 1179 | 1439 | 1710 |
| Adiabat | 1.000 | 0.8687 | 0.8276 | 0.7939 | 0.7650 | 0.7400 | 0.7180 | 0.6983 | 0.6800 | 0.6624 |
| T_A | 20°C | 99 | 124 | 144 | 163 | 181 | 195 | 210 | 223 | 233 |
| Adiabat (474 kilobars) | 1.002 | 0.8969 | 0.8507 | 0.8142 | 0.7833 | 0.7566 | 0.7336 | 0.7124 | 0.6936 | 0.6760 |
| T_A | 1055°C | 1157 | 1242 | 1314 | 1381 | 1439 | 1495 | 1547 | 1593 | |
| Niobium | | | | | | | | | | |
| 0°K | 0.9951 | 0.9440 | 0.9226 | 0.9032 | 0.8856 | 0.8694 | 0.8544 | 0.8404 | 0.8271 | 0.8148 |
| Hugoniot | 1.000 | 0.9476 | 0.9260 | 0.9067 | 0.8894 | 0.8730 | 0.8582 | 0.8449 | 0.8321 | 0.8197 |
| T_H | 20°C | 49 | 73 | 97 | 133 | 177 | 227 | 284 | 351 | 427 |
| Adiabat | 1.000 | 0.9475 | 0.9256 | 0.9061 | 0.8885 | 0.8721 | 0.8566 | 0.8427 | 0.8296 | 0.8171 |
| T_A | 20°C | 45 | 55 | 65 | 73 | 81 | 89 | 96 | 103 | 110 |
| Adiabat (528 kilobars) | 1.006 | 0.9526 | 0.9302 | 0.9104 | 0.8923 | 0.8756 | 0.8601 | 0.8459 | 0.8326 | 0.8200 |
| T_A | 287°C | 335 | 358 | 377 | 393 | 409 | 424 | 439 | 452 | 465 |
| Palladium | | | | | | | | | | |
| 0°K | 0.9918 | 0.9422 | 0.9233 | 0.9071 | 0.8930 | 0.8808 | 0.8696 | 0.8596 | 0.8500 | 0.8410 |
| Hugoniot | 1.000 | 0.9520 | 0.9330 | 0.9170 | 0.9029 | 0.8903 | 0.8792 | 0.8692 | 0.8600 | 0.8513 |
| T_H | 20°C | 65 | 97 | 135 | 180 | 231 | 289 | 353 | 423 | 497 |
| Adiabat | 1.000 | 0.9517 | 0.9326 | 0.9159 | 0.9011 | 0.8882 | 0.8766 | 0.8658 | 0.8556 | 0.8466 |
| T_A | 20°C | 61 | 79 | 104 | 125 | 143 | 159 | 177 | 192 | 205 |
| Adiabat (481 kilobars) | 1.006 | 0.9587 | 0.9399 | 0.9230 | 0.9080 | 0.8941 | 0.8820 | 0.8710 | 0.8609 | 0.8512 |
| T_A | 187°C | 246 | 278 | 311 | 343 | 375 | 403 | 429 | 454 | 477 |
| Platinum | | | | | | | | | | |
| 0°K | 0.9940 | 0.9632 | 0.9500 | 0.9377 | 0.9260 | 0.9154 | 0.9052 | 0.8959 | 0.8868 | 0.8779 |
| Hugoniot | 1.000 | 0.9679 | 0.9540 | 0.9412 | 0.9298 | 0.9190 | 0.9087 | 0.8993 | 0.8903 | 0.8819 |
| T_H | 20°C | 46 | 60 | 77 | 95 | 117 | 144 | 174 | 207 | 244 |
| Adiabat | 1.000 | 0.9678 | 0.9539 | 0.9410 | 0.9292 | 0.9183 | 0.9081 | 0.8985 | 0.8891 | 0.8806 |
| T_A | 20°C | 44 | 54 | 63 | 71 | 78 | 85 | 91 | 97 | 102 |
| Adiabat (481 kilobars) | 1.003 | 0.9697 | 0.9567 | 0.9429 | 0.9310 | 0.9199 | 0.9096 | 0.8999 | 0.8905 | 0.8819 |
| T_A | 119°C | 151 | 165 | 177 | 187 | 197 | 207 | 216 | 224 | 231 |

TABLE IV.—Continued.

| P (kilobars) | 0 | 100 | 150 | 200 | 250 | 300 | 350 | 400 | 450 | 500 |
|------------------|--------|--------|--------|--------|--------|--------|--------|--------|--------|--------|
| Rhodium | | | | | | | | | | |
| 0°K | 0.9946 | 0.9642 | 0.9509 | 0.9380 | 0.9264 | 0.9156 | 0.9053 | 0.8958 | 0.8864 | 0.8778 |
| Hugoniot | 1.000 | 0.9683 | 0.9548 | 0.9419 | 0.9301 | 0.9191 | 0.9090 | 0.8992 | 0.8899 | 0.8812 |
| T_H | 20°C | 42 | 54 | 69 | 85 | 104 | 127 | 153 | 181 | 218 |
| Adiabatic | 1.000 | 0.9683 | 0.9545 | 0.9417 | 0.9299 | 0.9188 | 0.9081 | 0.8982 | 0.8889 | 0.8802 |
| T_A | 20°C | 41 | 48 | 56 | 64 | 71 | 77 | 83 | 89 | 97 |
| Adiabatic | | | | | | | | | | |
| (478 kilobars) | 1.002 | 0.9698 | 0.9561 | 0.9432 | 0.9311 | 0.9200 | 0.9095 | 0.8998 | 0.8901 | 0.8811 |
| T_A | 106°C | 133 | 144 | 155 | 165 | 173 | 181 | 189 | 197 | 204 |
| Tantalum | | | | | | | | | | |
| 0°K | 0.9952 | 0.9463 | 0.9273 | 0.9089 | 0.8921 | 0.8768 | 0.8622 | 0.8489 | 0.8363 | 0.8244 |
| Hugoniot | 1.000 | 0.9510 | 0.9307 | 0.9122 | 0.8955 | 0.8803 | 0.8657 | 0.8524 | 0.8400 | 0.8284 |
| T_H | 20°C | 47 | 69 | 92 | 121 | 160 | 207 | 260 | 315 | 379 |
| Adiabatic | 1.000 | 0.9510 | 0.9304 | 0.9119 | 0.8951 | 0.8795 | 0.8649 | 0.8510 | 0.8383 | 0.8264 |
| T_A | 20°C | 45 | 55 | 61 | 70 | 79 | 86 | 93 | 99 | 106 |
| Adiabatic | | | | | | | | | | |
| (540 kilobars) | 1.005 | 0.9555 | 0.9345 | 0.9156 | 0.8983 | 0.8827 | 0.8680 | 0.8539 | 0.8411 | 0.8290 |
| T_A | 272°C | 314 | 336 | 354 | 369 | 383 | 397 | 410 | 423 | 435 |
| Thallium | | | | | | | | | | |
| 0°K | 0.8446 | 0.8229 | 0.7850 | 0.7558 | 0.7314 | 0.7117 | 0.6937 | 0.6782 | 0.6642 | 0.6510 |
| Hugoniot | 1.000 | 0.8440 | 0.8063 | 0.7785 | 0.7558 | 0.7368 | 0.7203 | 0.7063 | 0.6940 | 0.6822 |
| T_H | 20°C | 315 | 531 | 791 | 1079 | 1392 | 1719 | 2105 | 2447 | 2831 |
| Adiabatic | 1.000 | 0.8387 | 0.7987 | 0.7672 | 0.7416 | 0.7200 | 0.7016 | 0.6849 | 0.6708 | 0.6578 |
| T_A | 20°C | 192 | 248 | 293 | 333 | 367 | 398 | 425 | 450 | 473 |
| Adiabatic | | | | | | | | | | |
| (489 kilobars) | 1.097 | 0.9072 | 0.8542 | 0.8142 | 0.7822 | 0.7557 | 0.7335 | 0.7141 | 0.6969 | 0.6817 |
| T_A | 671°C | 1383 | 1656 | 1181 | 2076 | 2247 | 2401 | 2534 | 2657 | 2769 |
| Zirconium | | | | | | | | | | |
| 0°K | 0.9968 | 0.9068 | 0.8709 | 0.8394 | 0.8112 | 0.7860 | 0.7629 | 0.7420 | 0.7227 | 0.7049 |
| Hugoniot | 1.000 | 0.9098 | 0.8739 | 0.8421 | 0.8144 | 0.7894 | 0.7670 | 0.7467 | 0.7280 | 0.7104 |
| T_H | 20°C | 55 | 92 | 143 | 214 | 298 | 395 | 503 | 616 | 737 |
| Adiabatic | 1.000 | 0.9090 | 0.8733 | 0.8414 | 0.8131 | 0.7879 | 0.7646 | 0.7435 | 0.7244 | 0.7062 |
| T_A | 20°C | 41 | 50 | 59 | 67 | 75 | 81 | 88 | 94 | 99 |
| Adiabatic | | | | | | | | | | |
| (459 kilobars) | 1.008 | 0.9159 | 0.8792 | 0.8470 | 0.8182 | 0.7925 | 0.7690 | 0.7480 | 0.7281 | 0.7100 |
| T_A | 447°C | 502 | 526 | 547 | 565 | 584 | 601 | 618 | 633 | 647 |

ments were made) for which the calculations indicate melting in the present experimental range. Shock waves just strong enough for incipient melting of lead, tin, and cadmium (initially at 20°C) are 245 kilobars, 225 kilobars, and 325 kilobars, respectively. For stronger shock waves, at least partial melting occurs as the material is relieved to zero pressure. Melting phenomena are not included in any of the calculations of the present paper.

24ST aluminum data for hydrodynamic applications are listed in Tables VI and VII. The calculations were carried out by the methods outlined above and did incorporate the refinement of the free-surface velocity approximation.

SUMMARIZING REMARKS

Shock-wave experiments were performed to determine Hugoniot curves to pressures of several hundred kilobars. The Hugoniot curves, the Mie-Grüneisen equation of state, and the Dugdale-MacDonald formula were then employed to calculate complete thermodynamic descriptions of the various metals, for states neighboring the experimental curves. The calculated offsets between the Hugoniot curves and neighboring $P-V$

TABLE V. Ratio of the Riemann integral to the shock wave particle velocity, as a function of shock pressure.

| Metal | 100 kilobars | 300 kilobars | 500 kilobars |
|---------------|--------------|--------------|--------------|
| Beryllium | 1.000 | 1.003 | |
| Cadmium | 1.005 | 1.031 | melting |
| Chromium | 1.000 | 1.000 | 1.001 |
| Cobalt | 1.000 | 1.003 | 1.008 |
| Copper | 1.001 | 1.005 | 1.012 |
| Gold | 1.000 | 1.006 | 1.016 |
| Lead | 1.009 | melting | melting |
| Magnesium | 1.005 | 1.027 | |
| Molybdenum | 1.000 | 1.001 | 1.002 |
| Nickel | 1.000 | 1.003 | 1.007 |
| Silver | 1.002 | 1.011 | 1.024 |
| Thorium | 1.001 | 1.010 | 1.022 |
| Tin | 1.003 | melting | melting |
| Titanium | 1.000 | 1.002 | 1.006 |
| Zinc | 1.004 | 1.022 | 1.042 |
| 24ST aluminum | 1.003 | 1.015 | 1.030 |
| Brass | 1.001 | 1.009 | 1.019 |
| Indium | 1.008 | melting | melting |
| Niobium | 1.000 | 1.003 | 1.007 |
| Palladium | 1.000 | 1.004 | 1.009 |
| Platinum | 1.001 | 1.003 | 1.006 |
| Rhodium | 1.000 | 1.002 | 1.005 |
| Tantalum | 1.000 | 1.002 | 1.005 |
| Thallium | 1.014 | melting | melting |
| Zirconium | 1.000 | 1.001 | 1.003 |

TABLE VI. Shock wave parameters for 24ST aluminum.

| Shock wave pressure P (kilobars) | Relative volume V/V_0 | Shock wave velocity U_s km/sec | Shock particle velocity U_p km/sec | Sound speed C km/sec | Temperature T °C |
|---------------------------------------|-------------------------|-------------------------------------|---|---------------------------|-----------------------|
| 100 | 0.9043 | 6.125 | 0.571 | 6.307 | 99 |
| 125 | 0.8873 | 6.305 | 0.712 | 6.497 | 125 |
| 150 | 0.8716 | 6.475 | 0.831 | 6.667 | 154 |
| 175 | 0.8573 | 6.640 | 0.947 | 6.825 | 187 |
| 200 | 0.8441 | 6.793 | 1.057 | 6.970 | 223 |
| 225 | 0.8322 | 6.940 | 1.165 | 7.106 | 264 |
| 250 | 0.8210 | 7.082 | 1.267 | 7.233 | 308 |
| 275 | 0.8104 | 7.220 | 1.368 | 7.348 | 356 |
| 300 | 0.8008 | 7.350 | 1.465 | 7.465 | 406 |
| 325 | 0.7912 | 7.476 | 1.561 | 7.624 | 460 |
| 350 | 0.7824 | 7.598 | 1.654 | 7.675 | 516 |
| 375 | 0.7740 | 7.718 | 1.744 | 7.771 | 576 |
| 400 | 0.7661 | 7.836 | 1.832 | 7.862 | 637 |
| 425 | 0.7585 | 7.950 | 1.920 | 7.948 | 702 |
| 450 | 0.7513 | 8.062 | 2.003 | 8.032 | 768 |
| 475 | 0.7445 | 8.171 | 2.082 | 8.112 | 837 |
| 500 | 0.7380 | 8.276 | 2.170 | 8.190 | 907 |

curves of interest are generally small, only a few percent in compression. Hence, despite the approximations inherent in the Mie-Grüneisen and Dugdale-MacDonald equations, errors arising in the P - V curves due to the calculations are probably only comparable to uncertainties in the experimental data.

The important question of equivalence for the shock-wave results and laboratory pressure-volume data is perhaps best evaluated by examination of the data plots, Figs. 3 to 29. For most metals, the compatibility, if judged by downward extrapolation of the analytical fits, is quite good. This is especially true of comparisons

TABLE VII. Pressure *versus* particle velocity curves for 24ST aluminum. Each number in parentheses is a particle velocity (km/sec) for the corresponding shock pressure (kilobars). Remaining numbers in a given column then trace out the associated cross curve (see Fig. 2 and Section IB).

| P | Particle velocity | | | | | | | | | |
|-----|-------------------|---------|---------|---------|---------|---------|---------|---------|---------|-----|
| 0 | 1.165 | 1.655 | 2.098 | 2.576 | 2.945 | 3.380 | 3.680 | ... | ... | ... |
| 100 | (0.571) | 1.075 | 1.775 | 1.960 | 2.345 | 2.750 | 3.082 | 3.445 | ... | ... |
| 150 | 0.342 | (0.831) | 1.285 | 1.707 | 2.100 | 2.493 | 2.833 | 3.188 | 3.613 | ... |
| 200 | 0.118 | 0.606 | (1.057) | 1.480 | 1.875 | 2.260 | 2.605 | 2.958 | 3.375 | ... |
| 250 | ... | 0.400 | 0.848 | (1.267) | 1.662 | 2.042 | 2.394 | 2.744 | 3.130 | ... |
| 300 | ... | 0.203 | 0.652 | 1.066 | (1.465) | 1.844 | 2.195 | 2.543 | 2.950 | ... |
| 350 | ... | 0.008 | 0.465 | 0.880 | 1.280 | (1.654) | 2.010 | 2.352 | 2.688 | ... |
| 400 | ... | ... | 0.290 | 0.700 | 1.107 | 1.473 | (1.832) | 2.177 | 2.507 | ... |
| 450 | ... | ... | 0.120 | 0.527 | 0.935 | 1.302 | 1.662 | (2.003) | 2.337 | ... |
| 500 | ... | ... | ... | 0.364 | 0.765 | 1.136 | 1.500 | 1.838 | (2.170) | ... |

with the recent measurements to 30 kilobars by Professor Bridgman. Several of the static measurements to 100 kilobars, however, indicate compressions which are a few percent smaller than the corresponding shock wave results. In regard to the latter comparisons, it should be noted that the approximate nature of either of the present basic assumptions (thermal equilibrium and isotropy) would cause the shock wave results to indicate too little compression, and hence is not in the desired direction to account for the small observed offsets.

ACKNOWLEDGMENTS

The present effort was made possible only through the cooperation of a large number of people, most of whom are members of the GMX Division of the Los Alamos Scientific Laboratory.